Dynamics of a High RPM Hard Disk Drive in Operation State

B.H. Thornton and D.B. Bogy

Computer Mechanics Laboratory
Department of Mechanical Engineering
University of California, Berkeley 94720

***Abstract*—An investigation is presented of the dynamics associated with a high RPM hard disk drive (HDD) in its operation state in the bandwidth of 0-12kHz. Both finite element modeling (FEM) and analysis (FEA) and experimental methods are used. Initially, the major components of a HDD are modeled and validated with experiment. These models are combined together to create a FEM of a HDD and coupled modes and off-track modes are discussed. In order to incorporate rotational disks in the FEA, a coupled mode prediction of the disk and the actuator-suspension system is introduced and validated. Drive-level experimental modal analysis is performed and the results correlate well with FEA and the coupled mode prediction method. The results show that almost all structural modes are present in normal operation. Investigation into fly-height modulation and off-track or track misregistration (TMR) yield problematic structural resonances hindering reduction in fly-height and increasing track density. Spindle motor forces and windage created by the spinning disks are found to be the major causes of excitation under normal operation. In order to further decrease fly-height and track pitch, excitation sources must be suppressed and the major components must be modified.**

1. INTRODUCTION

In recent years the capacities of hard disk drives (HDD) has been doubling annually while holding the physical size of the drive constant- 1 inch and 1.6 inch form factors. This increase in capacity requires a higher areal density of bits stored on a disk. Also, the demand for a higher bit transfer rate and access time has led to increases in the disk rotational speed. These demands have decreased fly-height, increased tracks-per-inch (TPI), and increased spindle RPM. Near future fly-heights of 10nm, TPI of 100,000 and rotational speed of 20,000 RPM are expected. There is an increasing concern about the dynamics at the head disk interface (HDI) due to mechanical vibrations. Disk diameters have decreased from the traditional 3.5 inches to 3 or 2.5 inches, decreasing the area per platter. Also substrates have changed and disks are thicker. By increasing the spindle speed, decreasing the fly-height, and increasing TPI, the fly-height modulation and track misregistration (TMR) or off-track modulation becomes more of a concern. Smaller variations in lateral and transverse vibrations can potentially cause TMR and head slaps, respectively.

Many studies have been carried out at the component level for suspensions, spindle motors, and alternative disk substrates, but very few studies have been conducted at the system or drive level. Disk stack vibrations due to non symmetric disks, spindle motor excitations and windage created by the rotating disks has been shown to play a major roll in vibrations that cause TMR [1,3,4,8,9]. Due to ball-bearing runout and defects, fluid spindle bearing motors are being researched and they show promising results. Suspension design and windage effects on suspension vibrations have been studied

[10,11]. Also, alternative disk substrates have been shown to be effective in damping out vibrations.

The dynamics of a HDD are very complex. When dealing with very small structures and not very predictable forcing functions due to windage created by the spinning disks, ball bearing runout and defects in the spindle motor and other spindle motor forces, imbalance disk stacks, etc. the combined system is very complex to analyze. Through experimentation and finite element (FE) analysis this paper studies the interactions of the mechanical components in a 10,000 RPM HDD in the bandwidth of 0 to 12kHz. Specifically, we study the structural modes of vibration in normal operation and determine the modes contributing to fly-height modulation and off-track or TMR.

2. HARDWARE

This study was conducted using 10,020 RPM SCSI drives with specifications listed in table 1. These drives are full height (1.6 inch form factor) but have only 5 disks while most drives of this form factor have 10 or more disks. Also, the disks are 95 mm aluminum substrate disks similar to those of the previous generation HDD (7200 RPM).

3. COMPONENT LEVEL ANALYSIS

In order to better understand system dynamics, a thorough investigation of the systems mechanical components is needed. FEM/FEA is a very powerful tool for understanding structural modes and mode interactions of systems. In a HDD, several structures need to be taken into consideration when investigating dynamics. Some of the

components contributing to vibrations are the base casting, cover plate, ball-bearing spindle motor, disks, actuator E-block, and actuator/suspension system.

Due to the complexity of the modeling and the constraint on the number of nodes and elements that can be used in the model, some of the more difficult to model components or the less important components are not modeled here. In this paper, the FE analysis was used only for mode verification and a means to study how the modes interact when components are combined as a system. The suspension system (load beam, gimble, base plate, and slider), the actuator arm, and the disks were modeled. FE modal analysis was performed, and then compared to experimental modal analysis for verification of each component. All FE modeling and analysis was done using ANSYS55 software.

3.1 Slider-Suspension System

The load beam, gimble, base plate, and slider were modeled using 1002 shell 63 elements and 66 solid 45 elements as shown in figure 1. The slider was attached to the gimble through common nodes, the gimble to the load beam by coupled equations at the spot welds, and the load beam to the base plate through common nodes. The four corners of the slider were constrained in the z-direction and all degrees-of-freedom were constrained at the swage location as boundary conditions. FE modal analysis was performed on the suspension and the modes were solved for in the frequency band of 0-12kHz. The modal frequencies and shapes are summarized in table 2. The small tabs at the base end of the suspension have bending modes in the bandwidth of 0-12kHz, but since these modes do not contribute to the dynamics of the rest of the suspension system, they will no longer be referred to. The mode shapes in the bandwidth of 0-12kHz are shown in figure 2 in there deformed shape. The modes shapes found by FE analysis

contributing to off-track motion are shown in figure 3 in their deformed and undeformed shapes. An interesting result is that the first torsion mode does not significantly contribute to off-track motion of the slider.

In order to verify the FE model of the suspension, experimental modal analysis was performed. The suspension was unswaged from the actuator arm, the swage location of the slider was fixed and the suspension was loaded on the slider with a mechanical shaker in the z-direction. The input to the system was a random noise signal containing 0-12kHz exciting the system at the slider. The output was the velocity signal from a Polytec Scanning LDV scanned over the surface of the suspension arm and averaged 32 times. Figure 4 shows the average frequency response of the system. The modal frequencies and shapes were obtained using the Polytec animation software. Smaller bandwidths were then chosen in the bands of high mode densities to distinguish mode shapes and frequencies more accurately. Some of the modes found by experimental modal analysis were found not to be pure bending or pure torsion, possibly due to the non-symmetric leads glued to the side of the load beam, which was not taken into account in the FE model. Also, some of the modes were excited at very low amplitude, specifically the second and third torsion modes, making it difficult to compare experimental results with the finite element model. The FE and experimental analysis results are summarized in table 2 and good correlation between FE and experimental results is found.

3.2 Actuator

The actuator was modeled and modal analysis was performed. The solution from modal analysis showed many repeated modes coupling the actuator arms. In order to

reduce the number of modes in the FE analysis and to reduce the number of elements and nodes, the actuator was simplified to just the actuator arm alone as shown in figure 5. The actuator arm model consisted of 931 solid 72 elements. FE modal analysis of the actuator arm yielded similar modal shapes and frequencies of the actuator but with fewer modes because of the lack of coupling. By making this simplification certain modes of the E-block are not found with the FE model, specifically the so-called butterfly mode. A summary of the modal frequencies and shapes of the actuator arm are listed in table 3.

Experimental modal analysis was used for verification of the simplified FE model of the actuator. The actuator was fixed to a mechanical shaker at the pivot with an input of random noise excitation in the bandwidth of 0-12kHz. The output of the system was the velocity signal from a Polytec Scanning LDV of the scanned surface of the actuator arm averaged 32 times. The average frequency response is shown in figure 6 and the modal frequencies and shapes were found from animation software. Comparison of the FE and experimental analysis of the actuator arm is summarized in table 3. Similar to the study of the suspension, the modes of in-plane vibration such as sway, were not excited in this experiment. Good correlation was found between the FE model and experimental results.

3.3 Disk

A FE model was created of a 95 mm outer diameter, 25 mm inner diameter, 0.8 mm thick aluminum substrate disk with 728 solid 45 elements as shown in figure 7. The clamping at the ID (inner diameter) was simulated by constraining the nodes with a diameter of 31.6 mm or less to zero displacement. FE modal analysis was performed to find modal shapes and frequencies, and they are listed in table 4 and 5. The superscript

in $(m,n)^2$ denotes that there are two modes due to the symmetry of the disk for disk modes with one or more nodal diameters (n).

There are two effects that cause the disk modes to change frequencies for changing rotation speeds. First, there are the so called forward and backward traveling modes for the disk modes with one or more nodal diameters. The second effect is the stiffening of the disk due to centrifugal force. The forward w_{mn}^{F} and backward w_{mn}^{B} traveling modes are a well know phenomenon which can be predicted with the following equations:

$$w_{mn}^{B} = w_{nm}^{P} - n\Omega \qquad (1)$$

$$w_{mn}^{F} = w_{nm}^{P} + n\Omega \qquad (2)$$

Where:

1. (m,n) disk mode represents the shape of the mode (i.e. m nodal circle and n nodal diameters.
2. Ω represents the rotational speed of the disk.
3. w_{mn}^{P} is the natural frequency of the (m,n) mode measured from a reference frame on the spinning disk. The stiffening due to centrifugal stiffening is absorbed in this term.)

The first effect of mode frequencies shifting cannot be taken into account with ANSYS FE software, however the shift due to the second effect can be accounted for. With a prestress FE modal analysis, the frequency shifts can be found and are summarized in table 4. The frequency shifts due to the centrifugal force at a rotation speed of 10,000 RPM is at most 43.4 Hz where as the splitting of the large nodal diameter modes shifts the frequencies dramatically higher and lower. From the FE analysis and by use of equations (1) and (2) the predicted modes for the disk spinning at 10,000 RPM are summarized in table 4.

In order to measure the disk modes experimentally for the disk-stack, we used an impact hammer to excite the system. A FRF was measured between the impact hammer exciting the top disk near the middle diameter and the velocity response (LDV) of the top disk in the axial direction on the opposite side from the impact. The FRF (figure 8) yields information on the resonant frequencies but not the mode shapes. In order to obtain some mode shapes experimentally we created the so-called waterfall plot (figure 9). The waterfall plot is the properly scaled velocity spectra of the top disk at the OD (outer diameter) that shows how resonance changes as a function of the disk rotational speed. Frequency spectra were taken from 0-10kHz for the disk-stack assembly rotating in the range 1800-10,000 RPM in 100 RPM increments. The resonant peaks emanating from the origin (0 RPM, 0 Hz) that increase linearly with RPM as a function of frequency are axial disk runout from non-perpendicularities, clamping distortions, discrete excitations from the spindle motor and bearing geometry defects [1]. The resonant peaks emanating from the frequency axis are structural modes of the disk [1]. From the slopes of the resonance peaks on the waterfall plot and the use of equations (1) and (2), the disk modes (m,n) can be found exactly. Unfortunately, not all disk modes are vibrating with amplitude great enough to be seen on the waterfall plot so FE mode frequencies were compared to the FRF of the disk stack. An interesting result shows that the disk modes with one or more nodal circles, m, are not vibrating with a significant amplitude while the disk stack is spinning. Table 5 shows good correlation between the FE analysis and experimental results.

A waterfall plot was also created from the FE results with the information from the stiffening of the disk spinning at 10,000 RPM together with equations (1) and (2).

The results predicted the splitting of the modes as seen in figure 10. This plot will be used later for predicting the coupled modes of the drive system with spinning disks.

3.4 Results

The FE models were created for the simplified structural systems and compared to the actual components for verification of modal frequencies and shapes. The results show that relatively simple FE models of the components are able to model the dynamics of the actual components in the frequency band of 0-12kHz. More time could have been spent in creating models with less percent error in comparison to the experiments but the need for the FE models in this study was primarily to gain insight on the modes of the components, and the coupled modes in the system.

4. SYSTEM LEVEL ANALYSIS

4.1 Finite Element Model of the Drive

The drive under investigation consists of five disks and ten heads, each disk having a slider on each side. On the top and bottom disk, the actuator arms only have one suspension but all other actuator arms have two suspensions swaged onto it. Thus, there are two types of actuator-suspension systems: one-suspension swaged onto an actuator arm (1AS) and two-suspensions swaged onto an actuator arm (2AS) as seen in figure 11.

FE modal analysis was performed on the 1AS and 2AS arm-suspension systems, and the results show very different modal properties as summarized in table 6. The mode shape notation is as follows:

- Bi^{S}: The i^{th} bending mode of the suspension.
- Bi^{AS}: The i^{th} bending mode of the arm-suspension system.
- Ti^{S}: The i^{th} torsion mode of the suspension.

- Ti^{AS}: The i^{th} torsion mode of the arm-suspension system.
- The (+) and (-) in the superscript for the 2AS system denotes in-phase (+) and out-of-phase (-)

The coupling between the suspension and actuator arm yield very interesting and different modal properties when compared to the suspension alone. The results show that the major modes – bending, torsion, and sway couple together to form coupled arm-suspension modes. Also, some of the suspension modes are present without coupling with the actuator arm. The most noticeable result shows the 2AS system having more off-track contributing modes as compared to the 1AS system in the bandwidth of 0-12kHz, as can be seen as highlighted modes in table 6. Figures 12 and 13 depict the mode shapes and frequencies contributing most to off-track motion.

To simplify the FE model of the HDD several assumptions were made:

(a) Base casting and cover plate vibrations are negligible.
(b) Spindle motor dynamics are very complex and are neglected.
(c) Actuator dynamics can be modeled by separate actuator arms.

Assumption (a) was made to reduce the number of nodes and elements of relatively large, stiff components. Assumption (b) was made to reduce to modeling time of the system. Many research papers have been written on just the dynamics of spindle bearing motors and liquid bearing motors, and they show complex dynamics [3,4,8,9]. Bearing defects, together with the disk stack whirling mode coupled with the (0,1) disk mode contributes to dynamics and, possibly, in future FE models the dynamics will be implemented [3,8,9]. Assumption (c) was made to reduce the number of modes due to coupling between the actuator arms. The "butterfly" and other E-block modes can contribute to off-track motion but they are neglected in the FE model. If extensive investigation of

HDD dynamics is done with stationary disks, such as shock studies, assumptions (a)-(c) could be implemented into a FE model [12].

The final FE model is shown in figure 14. The model consists of the following components:

⇒ Two Disks
⇒ Two 1AS arm-suspension systems
⇒ One 2AS arm-suspension system

The suspensions were attached to the actuator arms at the swage location with coupled equations coupling all degrees-of-freedom. The four corners of the sliders were attached to the disk by only coupling in the z-direction, which allows for relative motion over the surface of the disk. The entire system consisted of 42,978 degrees-of-freedom and modal analysis was performed on this system in the bandwidth of 0-12kHz. Approximately 120 modes were found of four general types:

⇒ Disk Modes
⇒ Suspension Modes
⇒ Arm-Suspension Modes
⇒ Disk/Arm-Suspension Coupled Modes

These results are similar to those found by Zeng and Bogy when investigating a 5400 RPM HDD [2]. There are many repeated modes due to symmetry of the system: symmetric disk modes and in-phase (+) and out-of-phase (-) arm-suspension system and disk modes. A summary of the system mode shapes and frequencies is shown in table 7. The following notation was used in summarizing the mode shapes:

- (m,n): m nodal circles, n nodal diameter disk mode.
- Bi^{ASj}: i^{th}-bending mode of the ASj actuator-suspension system.
- Ti^{ASj}: i^{th}-torsion mode of the ASj actuator-suspension system.
- In-phase and out-of-phase is denoted by a superscript (+) or (-) respectively.

An interesting result from the FEA of the disk drive system is that none of the modes contributing to off-track are coupled with the disk modes. Some of the off-track contributing modes are shown in figure 15. Figure 16 shows some coupled modes: $(1,2)^{+}B3^{S+/1S}B3^{S+/2S}$ at 4789.8 Hz and $(1,4)^{+}B4^{AS+/1S}B4^{AS+/2S}$ at 7067.8 Hz. Unfortunately the coupled modes with the stationary disk are not very useful for studying coupled modes with rotating disks due to the splitting of the disk modes with one or more nodal diameters. However, the results from the FEA of stationary disks can be used to predict which modes will couple with rotating disks.

An interesting result of the coupled modes with stationary disks shows that 1AS and 2AS arm-suspension and suspension bending modes that are close to a disk mode are coupled with the disk near the disk mode. This agrees with intuition of how the modes should interact and couple – the disks force the bending of the arm-suspension near the natural frequency of the bending modes. By using the waterfall plot generated by the FE model results for the disk (figure 10) and the FEA results of the 1AS and 2AS systems, a mode coupling prediction method can be obtained for rotating disks at 10,000 RPM. The waterfall plot shown in figure 17 has dashed lines representing the disk modes predicted by FE analysis and equations (1) and (2) and solid lines representing the structural modes of the 1AS system found by FE analysis. From this plot, it is seen that the 1AS bending modes have the potential to couple with the nearest disk mode. By this prediction method, we concluded that the following modes have the potential to couple at 10,000 RPM: $B1^{AS}(0,2)^{+}$ around 1110 Hz, $B1^{AS}(0,4)^{-}$ around 1304 Hz, $B2^{AS}(0,3)^{+}$ around 1711 Hz, $B2^{AS}(0,5)^{-}$ around 2175 Hz, $B3^{AS}(1,2)^{-}$ around 4490 Hz, $B3^{AS}(1,1)^{+}$ around 4462 Hz, $B3^{AS}(0,7)^{-}$ around 4728 Hz, $B4^{AS}(1,5)^{-}$ around 8131 Hz, $B4^{AS}(0,9)^{-}$ around 8486 Hz, and

$B4^{AS}(1,4)^{+}$ around 7791 Hz. The chance of the arm-suspension or suspension modes coupling with a disk mode with one or more nodal circles is small. The experimentally obtained waterfall plot shows that not all disk modes are substantially vibrating in the axial direction therefore those modes are less likely to couple with the arm-suspension system, especially the disk modes with one or more nodal circles. Also, from the FE analysis of the coupled modes, none of the torsion or sway modes coupled with the stationary disks; therefore it would be unlikely that they would couple with the spinning disks. These predicted coupled modes are summarized in table 9.

4.2 FEM Results

From FE analysis on the system of components, the modes of vibration can be found for stationary disks. When dealing with rotating disks, there at two factors that need to be taken into account – the so-called forward and backward traveling modes and the stiffening of the disk due to centrifugal force. The latter can be taken into account with the FE analysis and the former is taken into account with a predicted waterfall plot. Results from the FE modal analysis show very complex coupling. The bending modes of 1AS and 2AS are excited by the closest disk modes causing coupling, and the 1AS and 2AS show coupling between the actuator arm and the suspension. Also, a mode coupling prediction method for rotating disks at 10,000 RPM can be obtained as explained earlier to take into account the splitting of the disk modes with $n \neq 0$.

4.3 Experimental Setup for Modal Analysis

Any significant modification to the HDD could drastically modify its dynamic properties, so minimum modifications were done for making the measurements. Due to the configuration of the HDD under investigation, the only accessible arm-suspension system is the 1AS system. The drive has a bathtub base casting design with a steel cover plate. A hole cut in the steel cover plate exposed the 1AS system to allow access with LDV beams. A simple program was written in the C++ programming language to control the HDD via the SCSI with a PC controller. The program continuously reads logical block address (LBA) 0, which is the outer most data track. So, the condition simulated track following on an OD track. In order to perform the modal analysis to get the modal shapes and frequencies, we need an input to the system. To be consistent with the FE analysis constraining the clamped region of the disks and the base of the actuator arm to zero displacement, we take the pivot of the actuator as the reference point. The HDD was held rigidly and a single beam Polytec LDV was used for the input signal on the screw holding the pivot bearing of the actuator. This was the closest point accessible to the base of the actuator arm. The output signal was the velocity signal scanned over the 1AS system using a Scanning Polytec LDV.

4.4 Experimental Modal Analysis Results

An average frequency response is shown in figure 18. From this response curve and the Polytec mode animation software the modal frequencies and shapes can be found, and they are summarized in table 8. There were several mixed modes of vibration that caused difficulty in labeling the mode shapes, and they correspond to question marks in

the table summarizing the mode shapes. As can been seen from table 8, there are four different types of modes:

1) Strong 1AS modes
2) Strong disk modes
3) Strong suspension modes
4) Strong coupled modes

These results matched very well with the FEA and the coupled mode prediction method as can be seen in table 9. There are several peaks in the frequency response plot with similar modal frequencies and shapes. This could be a result of coupling between the E-block and/or manufacturing tolerances and imperfections shifting modal frequencies. Also the complexity of the multiple disk-stack could introduce some of this complex coupling. Another important result is that almost all the modes of vibration are excited under normal operation. It has been shown that windage created in a HDD is a broadband excitation, and this is the most likely cause for the structural resonances of the 1AS and 2AS modes [1].

4.5 Fly-Height Modulation: Experiment and Results

In order to measure the true fly-height modulation, we need to measure the change in the distance from the slider to the disk at the same lateral location. Unfortunately the suspension design is such that the slider is completely covered by the suspension load-beam; therefore the measurement is only an approximation of the fly-height modulation. A dual beam Polytec LDV was used for the measurement. One beam was focused on the backside of the suspension above the slider and the other beam was focused on the disk next to the slider. The output signal shown in figure 19 is both the

velocity and the displacement measurement of the approximate relative spacing variation. The measured displacement has relatively large amplitude – larger than the nominal fly-height of this drive, therefore it is not considered to be the actual fly-height modulation. However, its resonance peaks may lead to insight on the modes contributing to fly-height modulation. As seen from the frequency spectrum of the velocity signal of relative fly-height modulation in figure 19, the modes that possibly contribute to fly-height modulation are, in order of importance:

1. Bending modes of the arm-suspension and suspension.
2. Bending modes of the arm-suspension and suspension coupled with the disk.

The results from the experiment are as expected. The major contributors to fly-height modulation are the bending of the arm-suspension system and the suspension being excited, most likely, by windage forces. The second contributors are the coupled modes of the arm-suspension system and suspension with the disk modes being excited by windage and/or spindle motor forces and disk stack vibrations. Because the disk and the slider move largely together when coupled, the coupled modes do not contribute greatly to the fly-height modulation. The most difficult peak to explain is the strong first torsion mode. From FE analysis of the 1AS suspension system, we found that the first torsion mode of the suspension deforms very little in the transverse direction. Due to asymmetries in the suspensions caused by the lead wires glued on one side of the load beam, the modes are not pure (pure bending or pure torsion) but rather they are slightly mixed. This mixing of modes is not strong enough to create a strong response at the first torsional mode. A large peak suggests that the first torsion mode contributes to fly-height modulation, but this could be caused by the placement of the measurement LDV beam

off the center-of-mass of the slider, causing the torsion of the slider to appear as fly-height modulation. Summarizing the results leads us to conclude that the causes of fly-height modulation are windage forces, spindle motor forces and disk stack vibrations.

4.6 Off-Track Modulation: Experiment and Results

Vibrations of the slider in the radial direction of the disk is of major concern. This directly influences TMR and TPI. With increasing TPI, the ability to servo on a track becomes increasingly important. As track pitch becomes smaller, the allowable off-track vibration also becomes smaller. The goal is to find the modes contributing to off-track and suppress these amplitudes. In this paper we restrain the investigation to the modes that contribute to off-track errors.

The bathtub shape aluminum casting was removed and a hole was milled in the side of the casting to gain access to the sides of the sliders with the LDV beam. The experimental goal was to measure the velocity and displacement of the slider in the off-track direction while otherwise fixed on an OD track. Figure 20 shows both velocity and displacement of a 1AS systems slider in the off-track direction. A similar result for a 2AS system is shown in figure 21. The LDV signal was filtered with a high pass filter at 600 Hz to filter out the track following adjustments made by the servo system. The servo system has a bandwidth of approximately 600 Hz, therefore the frequency content above 600 Hz represents the uncontrollable off-track motion for this drive. The track density for this disk drive is approximately 9000 TPI, which translates to a 2.82μm track pitch. In order to minimize TMR, the allowable off-track displacement is on the order of 12% of the track pitch. Therefore, there is an allowable 0.3387μm of displacement of uncontrollable vibration. From the time domain data shown in figures 20 and 21, we see

that the vibration amplitude exceeds the envelope for allowable TMR. The main contributor to this displacement is the 8^{th} harmonic overtone of the disk rotational speed, 1336 Hz. The spindle motor is driven by 8 poles – hence it is pulsed 8 times per revolution, which induces this radial vibration.

An interesting result is that the first torsion mode contributes very little to off-track vibration. This result is consistent with the FEM results showing that the first torsion mode of the suspension is an out-of-plane motion. Structural modes contributing to the off-track vibration are the second torsion mode of the suspension and the sway modes and torsion modes of the arm-suspension system and disk modes. When discussing TMR and the contribution of specific causes of TMR, we often use the variance of off-track (σ^2). By plotting the position error signal (PES) in the frequency domain with units of [m^2/Hz] and integrating the area under the curve we obtain the variance of TMR [1]. Because the harmonic overtones of the disk rotational speed produce narrow peaks, the area under them is very small compared to that of the structural peaks with wider bandwidths, such as the second torsion modes. The structural modes contributing to off-track motion or TMR are listed in their order of importance as:

1) Torsion and Sway modes of the 1AS, 2AS and suspension systems.
2) Disk stack vibration modes.

It appears that the suspension design was successfully optimized to minimize the amplitude of the first torsion mode in the off-track direction. With the increasing bandwidth of servo systems it is becoming necessary to take into consideration in suspension design the other torsion modes and sway modes. Similar to the result from the fly-height modulation investigation, we find that the probable excitations exciting

these modes contributing to uncontrollable off-track vibrations are spindle motor forces, disk stack vibrations and windage forces.

5. Conclusion:

In this report, the dynamics associated with a high RPM HDD in the bandwidth of 0-12kHz was investigated under normal operation – specifically, under track following conditions. FE modeling and modal analysis was preformed for the major moving components of the drive, and this was validated with experimental modal analysis. The results show that fairly simple FE models can accurately capture the modal frequencies and shapes. These component FE models were then combined together and the dynamics of the HDD were found for the stationary disks. A coupled mode prediction method was introduced and used to predict the coupled modes for the disks spinning at 10k RPM. From the experimental modal analysis of the HDD under normal operation, we found the modal frequencies and shapes for the 1AS suspension system and disk stack. The results were consistent with the FE model of the HDD with stationary disks as well as the predicted coupled modes for rotating disks, and it was found that most of the modes are excited under normal operation.

Both fly-height and off-track modulation were found experimentally. Approximate measured fly-height modulation was attributed to the bending modes of the 1AS suspension system and the bending modes of the suspension alone. A second type of mode also contributed to the fly-height modulation, but with lower amplitude. These are the coupled modes of the bending of 1AS and suspension with the bending modes of the disk. Investigation of uncontrollable off-track vibrations revealed that the major causes of TMR to be the second and third torsion as well as the sway modes of the 1AS

and 2AS. The disk vibrations also caused TMR, but this was at a lower amplitude than the structural modes of the 1AS and 2AS systems.

In order to decrease the fly-height and increase TPI in future drives, we must reduce the modes contributing to fly-height and off-track modulation. From these results, it is seen that almost all modes of vibration are present under normal operation. These modes either must be damped to decrease their amplitudes and/or the excitation sources need to be decreased dramatically. Disk stack vibrations, windage created from the spinning disks and spindle motor forces are the major causes of excitation. A majority of the disk stack vibration is caused by windage due to the spinning of the disk, which in turn excites the arm-suspension systems and the suspensions. Alternative substrate disks and liquid bearing motors are being investigated in industry and are said to show promising results. Also, aerodynamic suspensions and actuators and shrouding may also be needed to provide possible solutions to these problems.

6. Acknowledgements

This study was supported by The Computer Mechanics Laboratory at the University of California, Berkeley. Special thanks go to IBM for supplying the HDD and for many helpful discussions with Dr. Rich Kroeker.

7. References

[1] McAllister, J. S. , 1996, "The Effect of Platter Resonances on Track Misregistration in Disk Drives", S/V Sound and Vibration, Jan. 1996, pp. 24-28.

[2] Zeng, Q. H., Bogy, D. B., "An Investigation of the Dynamic Characteristics of a Hard Disk Drive by Experiment and Analysis", CML report No. 96-017, Computer Mechanics Lab., Dept. of Mechanical Engineering, Univ. of California at Berkeley, August 1996.

[3] Frees, G.M., "Disk Drive Spindle Dynamics – Analysis and Measurement", ASME, Advances in Information Storage Systems, Vol. 6, 1996, pp.237-262.

[4] Zang, Y., Hatch, M.R., "On the Whirl Dynamics of Hydrodynamic Bearing Spindle in Information Storage Systems", ASME, ISPS, Vol. 2, 1996, pp.73-84.

[5] Miu, D.K., Frees, G.M., Gompertz, R.S., "Tracking Dynamics of Read/Write Head Suspensions in High-Performance Small Form Factor Rigid Disk Drives", Journal of Vibration and Acoustics, Vol. 112, Jan. 1990, pp.33-39.

[6] Huang, S.C., Chiou, W.J., "Modeling and Vibration Analysis of Spinning-Disk and Moving-Head Assembly in Computer Storage Systems", Journal of Vibration and Acoustics, Vol. 119, April 1997, pp.185-190.

[7] Chiou, S.S., Miu, D.K., "Tracking Dynamics of In-line Suspensions in High-Performance Rigid Disk Drives with Rotary Actuators", Journal of Vibration and Acoustics, Vol. 114, Jan. 1992, pp.67-72.

[8] Shen, I.Y., Ku, C.-P.R., "A Nonclassical Vibration Analysis of a Multiple Rotating Disk and Spindle Assembly", Journal of Applied Mechanics, Vol. 64, March 1997, pp.165-174.

[9] Shen, I.Y., "Closed-Form Forced Response of a Damped, Rotating, Multiple Disks/Spindle System", Journal of Applied Mechanics, Vol. 64, June 1997, pp.343-352.

[10] Kim, B.C., "The Effects of Unsteady Flow on the Slider Vibration in a Hard Disk Drive", CML report No. 99-014, Computer Mechanics Lab., Dept. of Mechanical Engineering, Univ. of California at Berkeley, August 1999.

[11] Kim, B.C., "Suppressing Turbulence Induced Vibration of the Head Suspension Assembly in a Hard Disk Drive", CML report No. 99-015, Computer Mechanics Lab., Dept. of Mechanical Engineering, Univ. of California at Berkeley, August 1999.

[12] Edwards, J.R., "Finite Element Analysis of the Shock Response and Head Slap Behavior of a Hard Disk Drive", IEEE Transactions on Magnetics, Vol. 35, No. 2, March 1999, pp. 863-867.

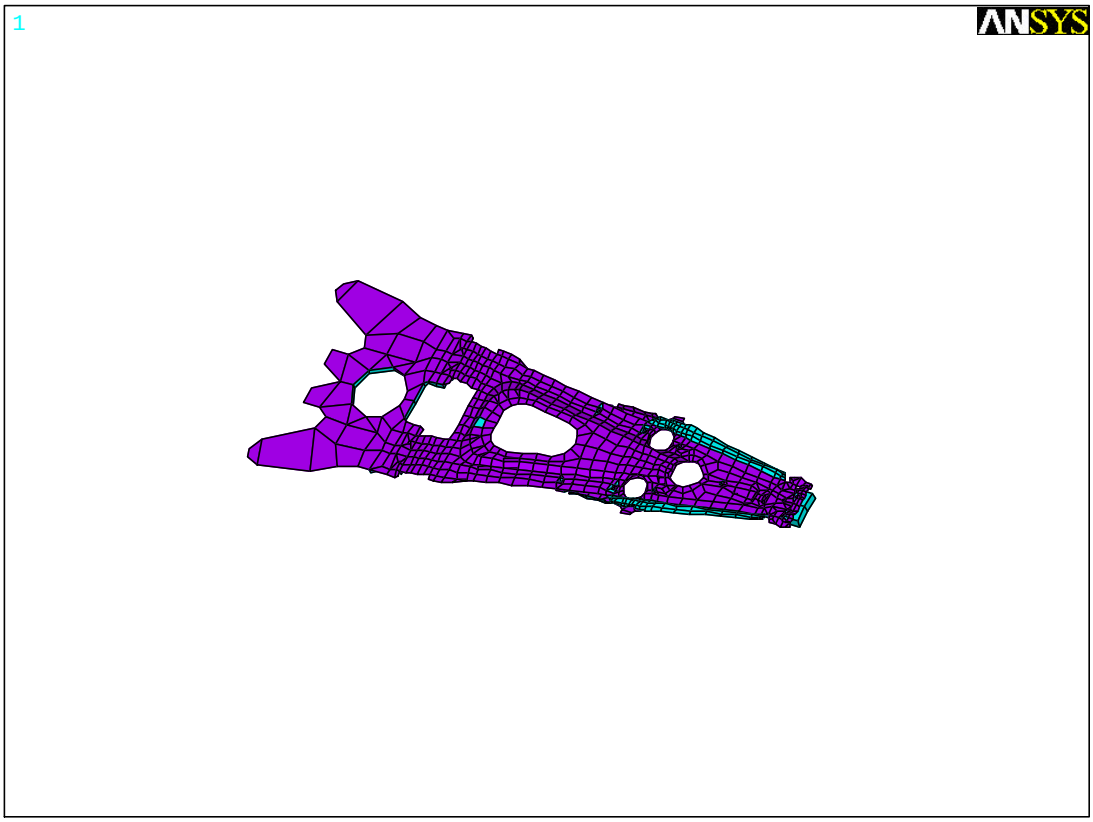

Figure 1: Finite element model of the suspension-slider system.

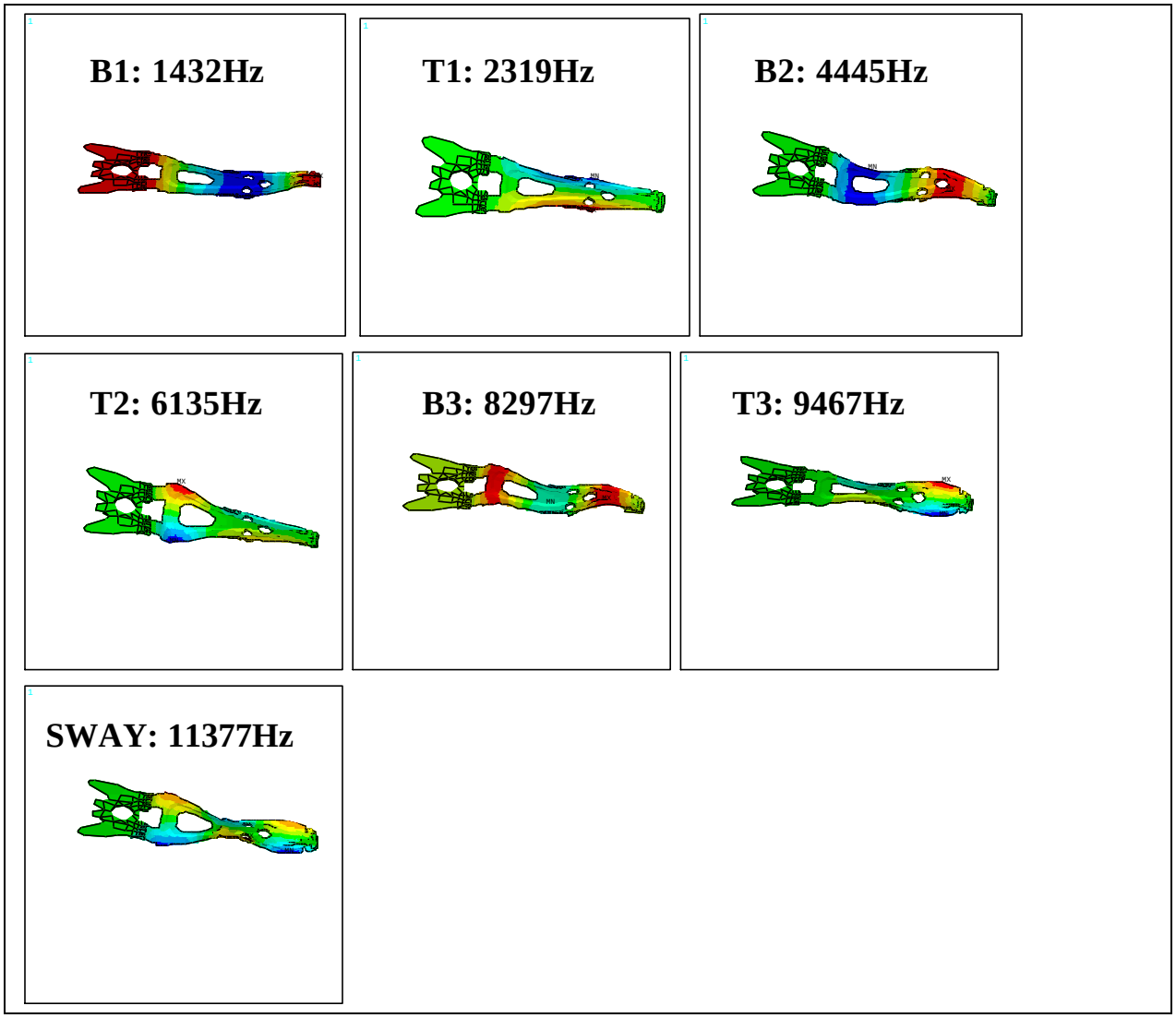

Figure 2: FE mode shapes of the suspension-slider system.

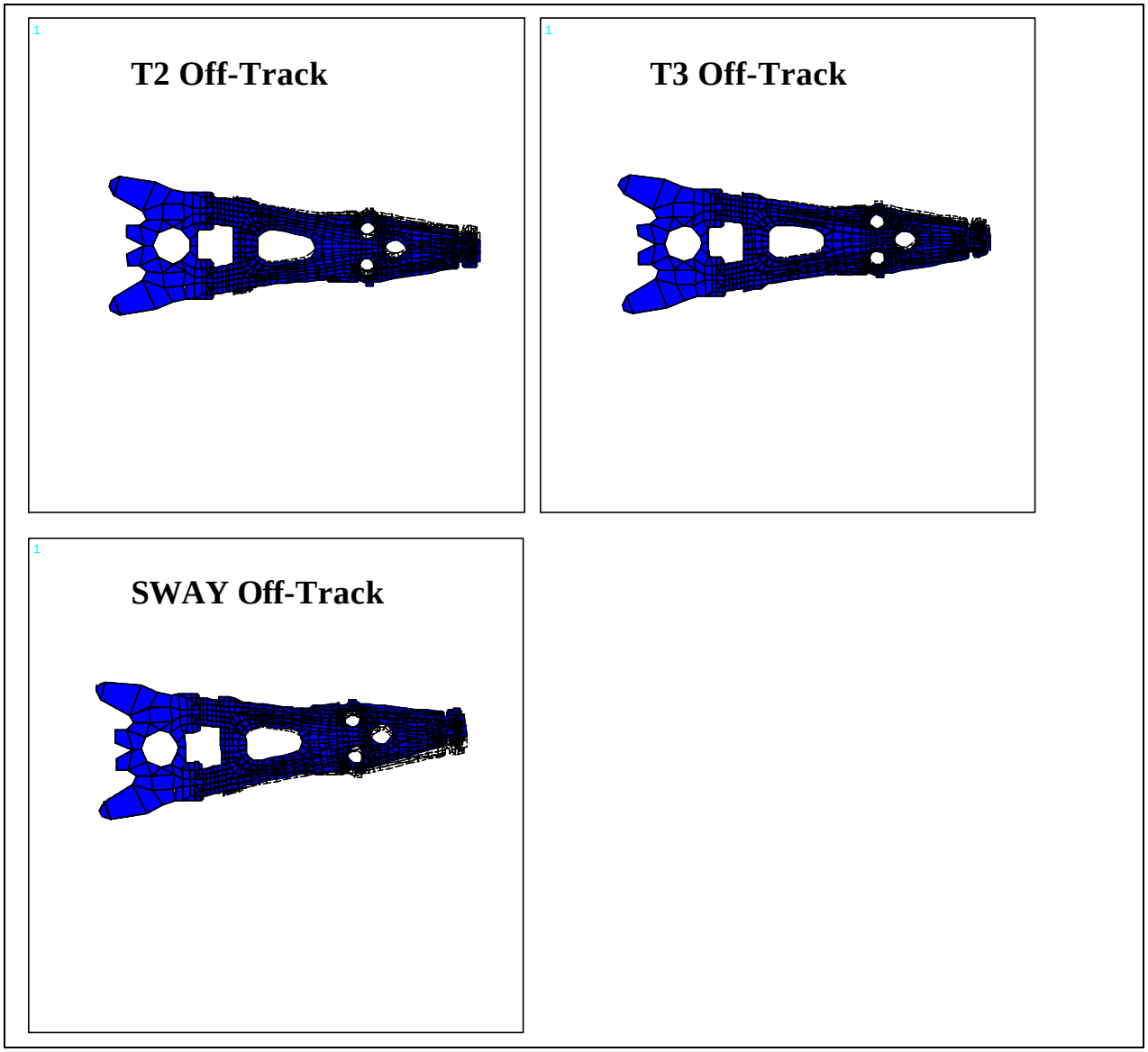

Figure 3: Deformed and undeformed modes contributing to off-track motion for the suspension-slider system.

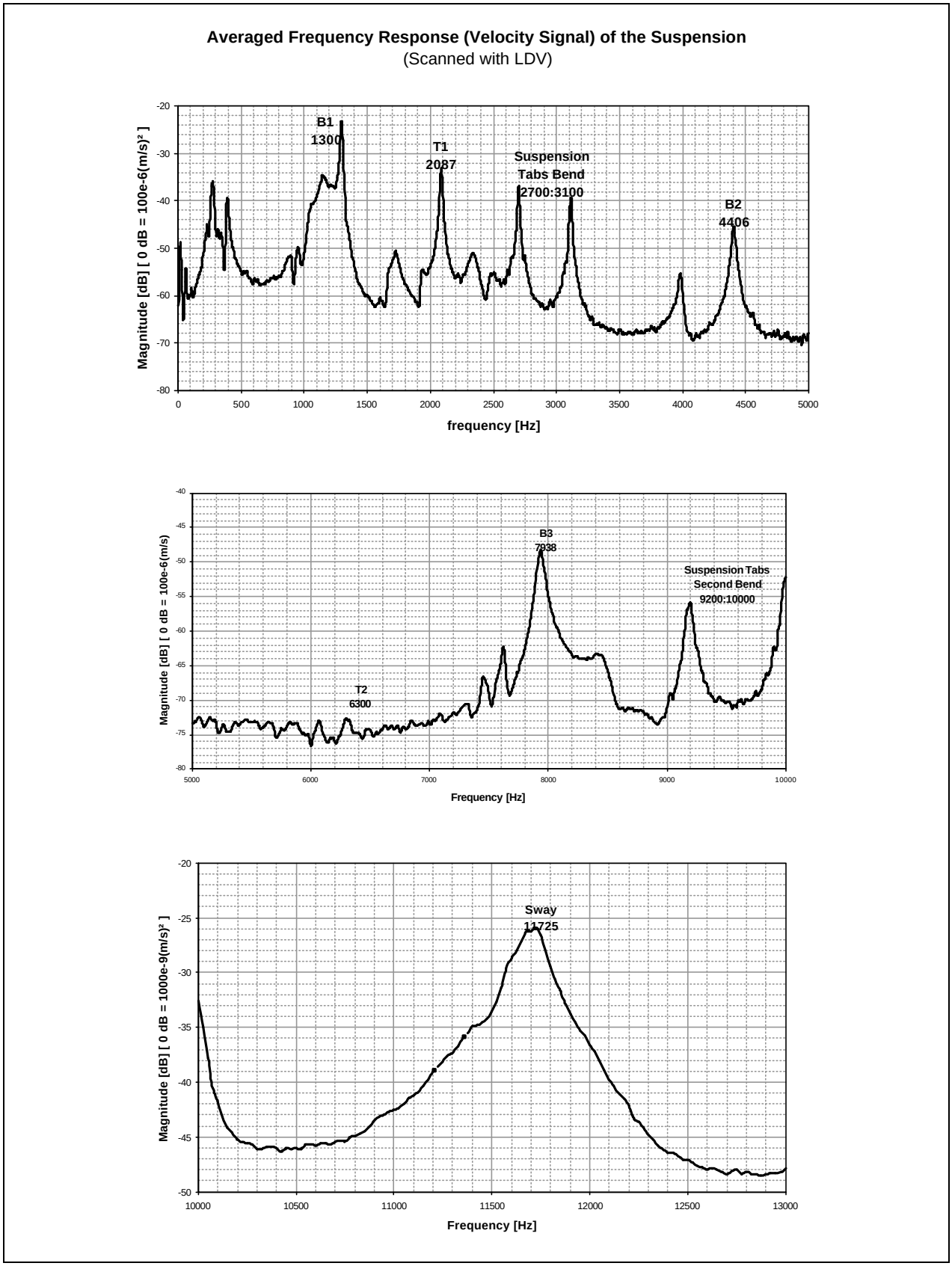

Figure 4: Averaged frequency response of the suspension-slider system from experimental modal analysis.

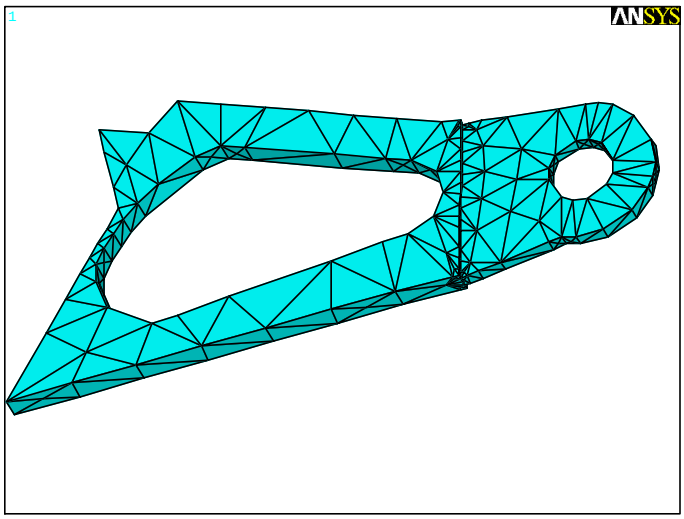

Figure 5: FE model of the actuator arm.

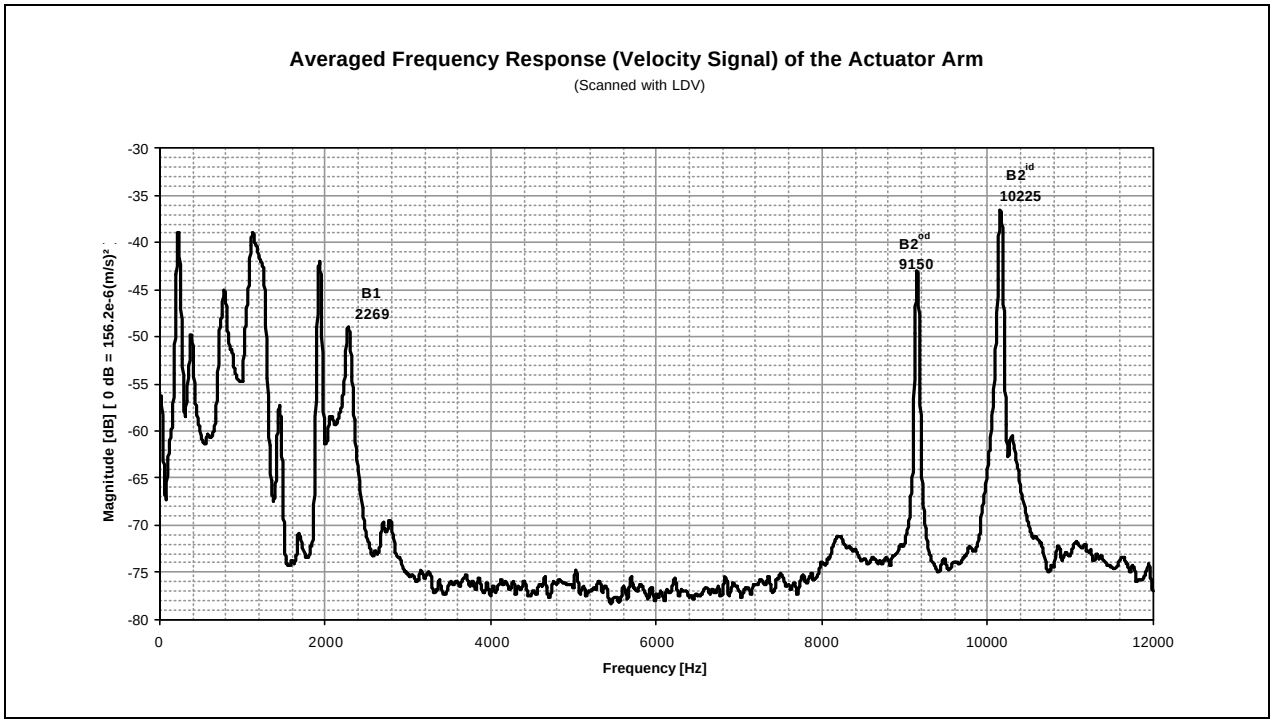

Figure 6: Averaged frequency response of the actuator arm from experimental modal analysis.

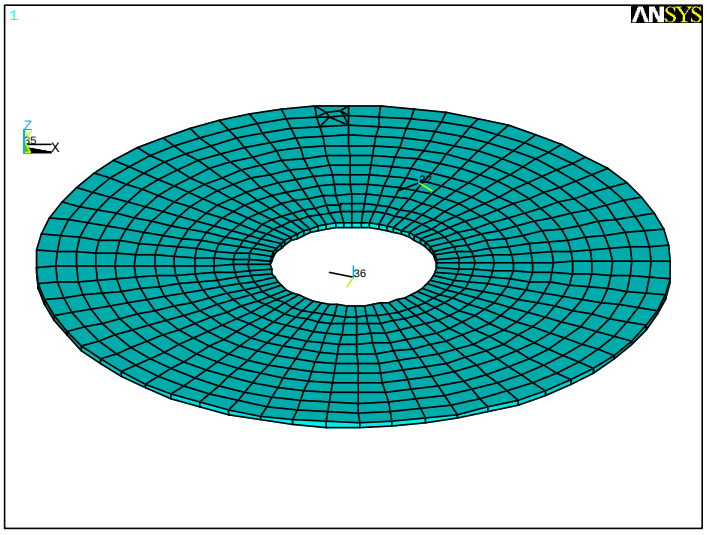

Figure 7: FE model of the disk.

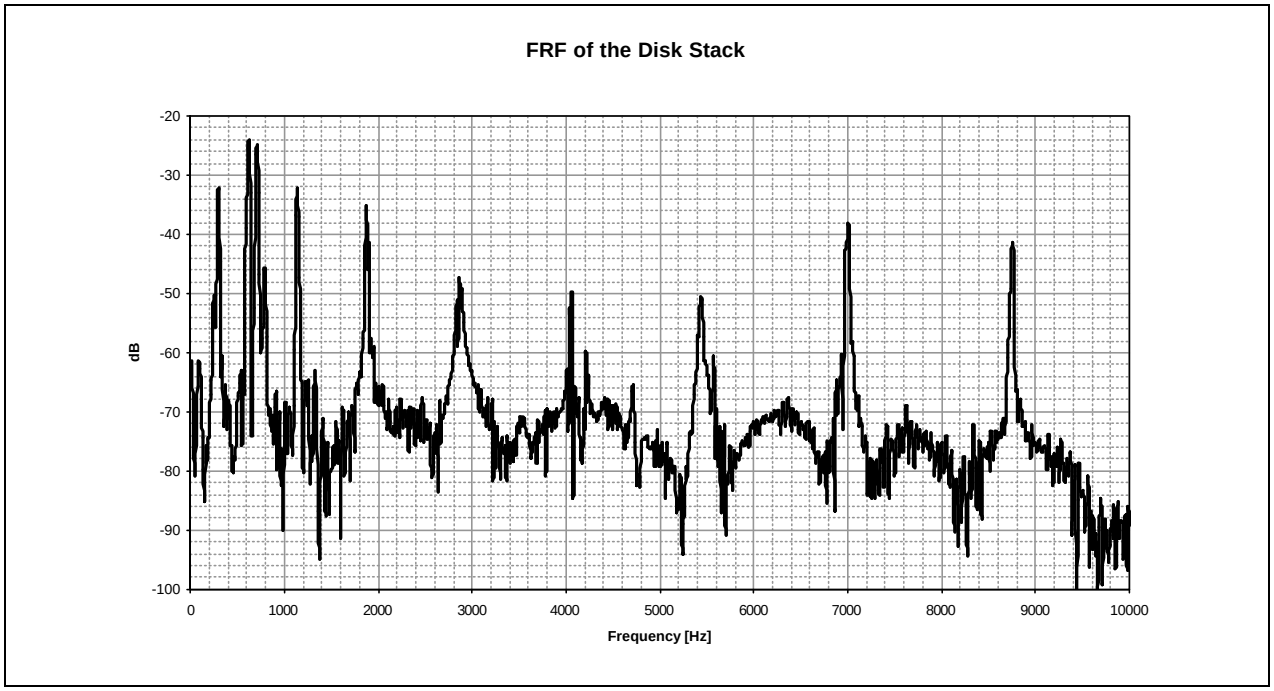

Figure 8: FRF of the disk stack excited with an impact hammer in the axial direction.

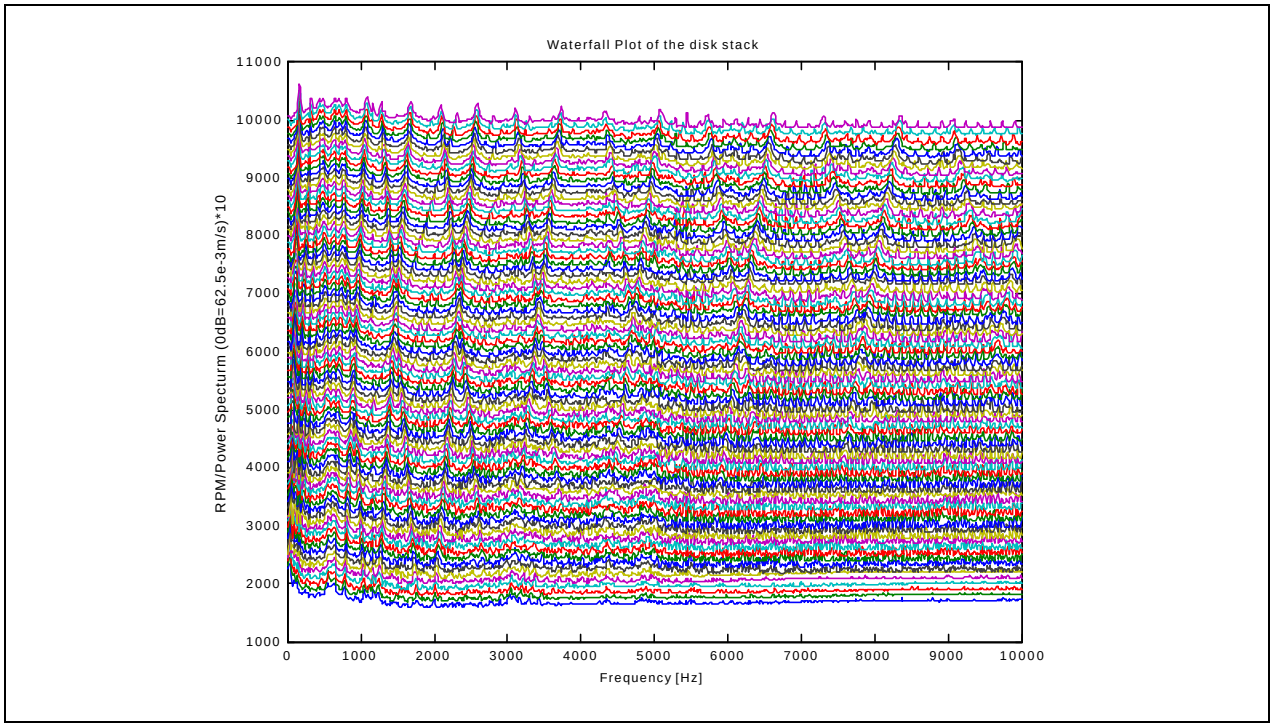

Figure 9: Experimental waterfall plot.

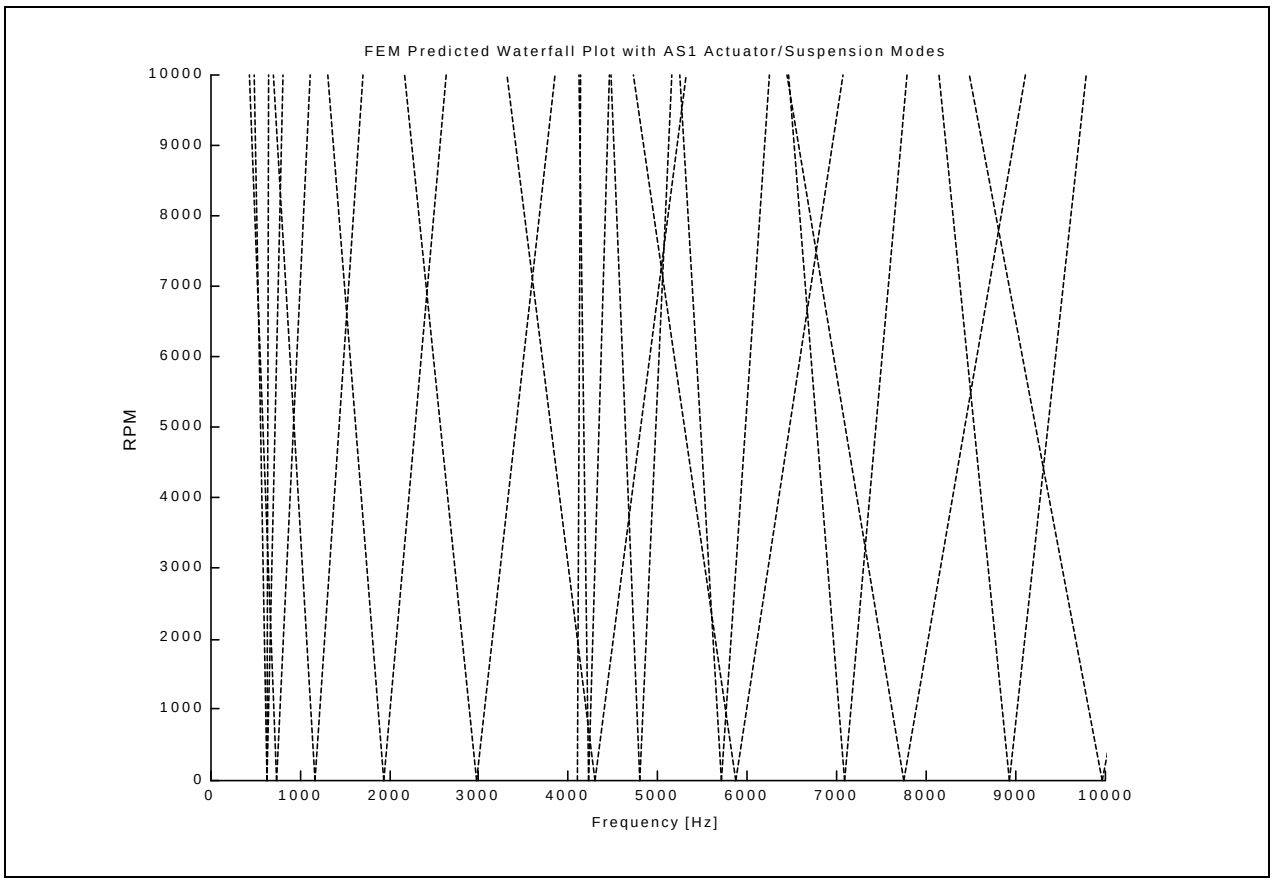

Figure 10: FE predicted waterfall plot.

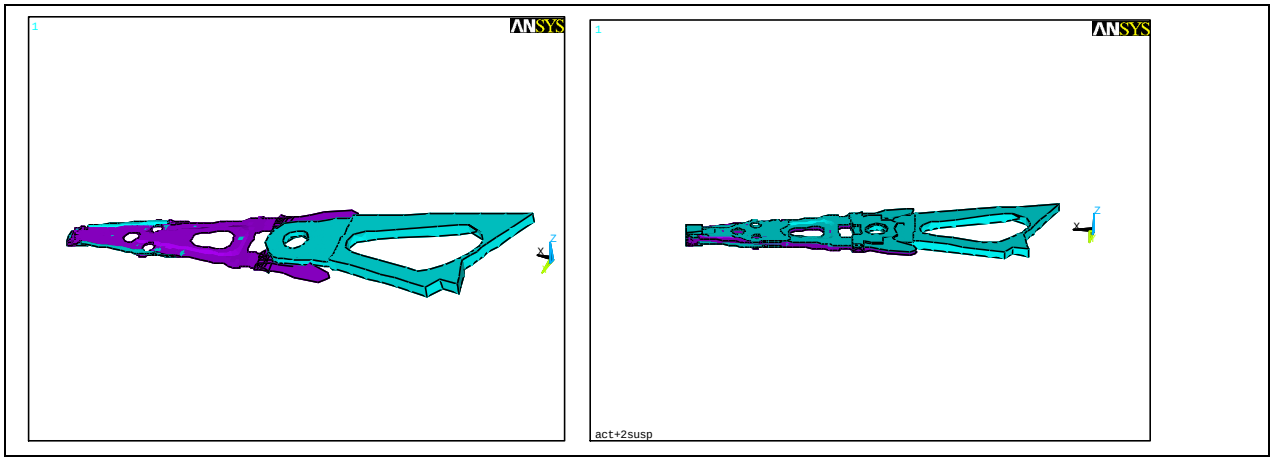

Figure 11: FE model of the 1AS & 2AS arm-suspension systems.

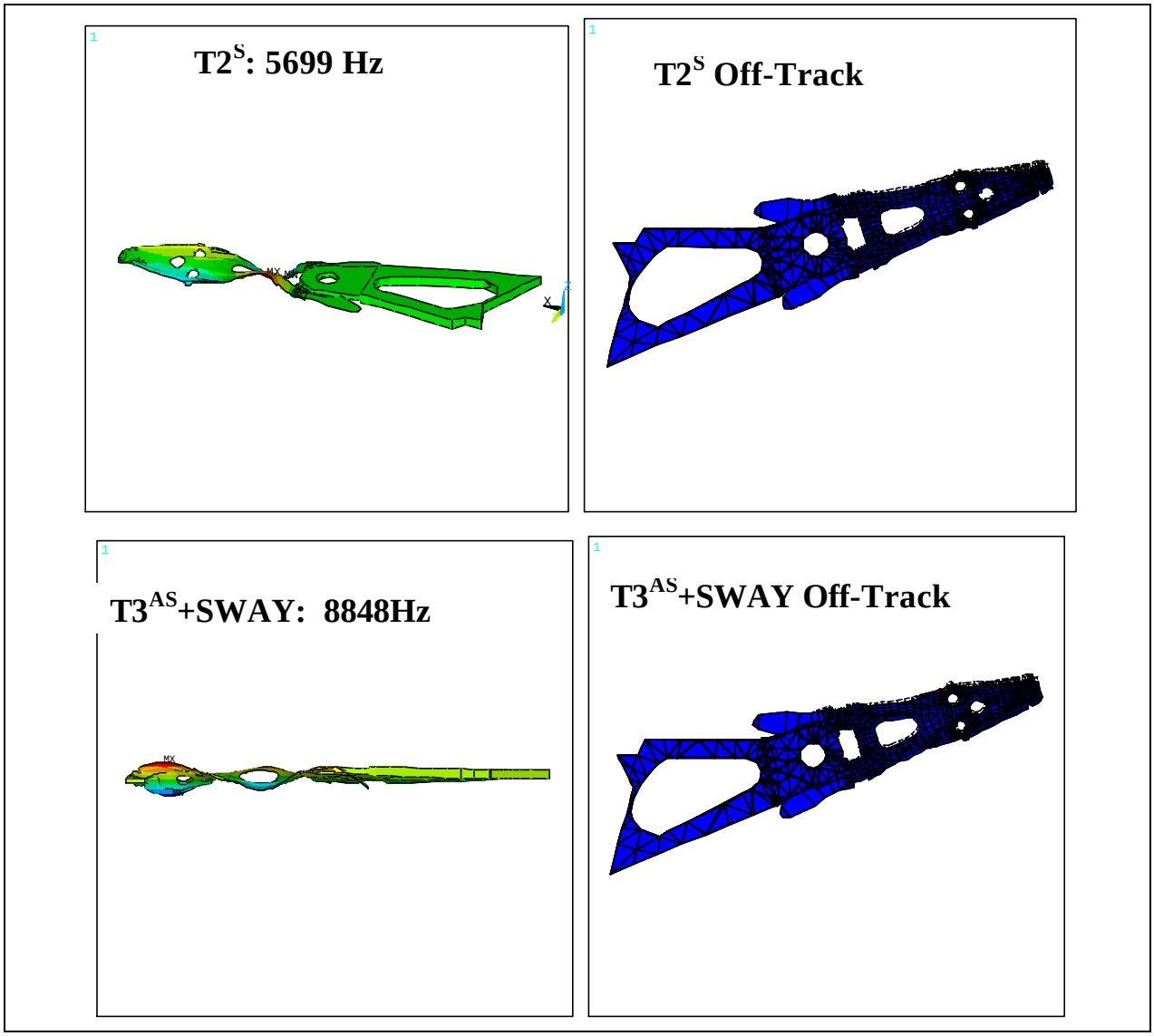

Figure 12: Modes contributing to off-track for the 1AS arm-suspension system.

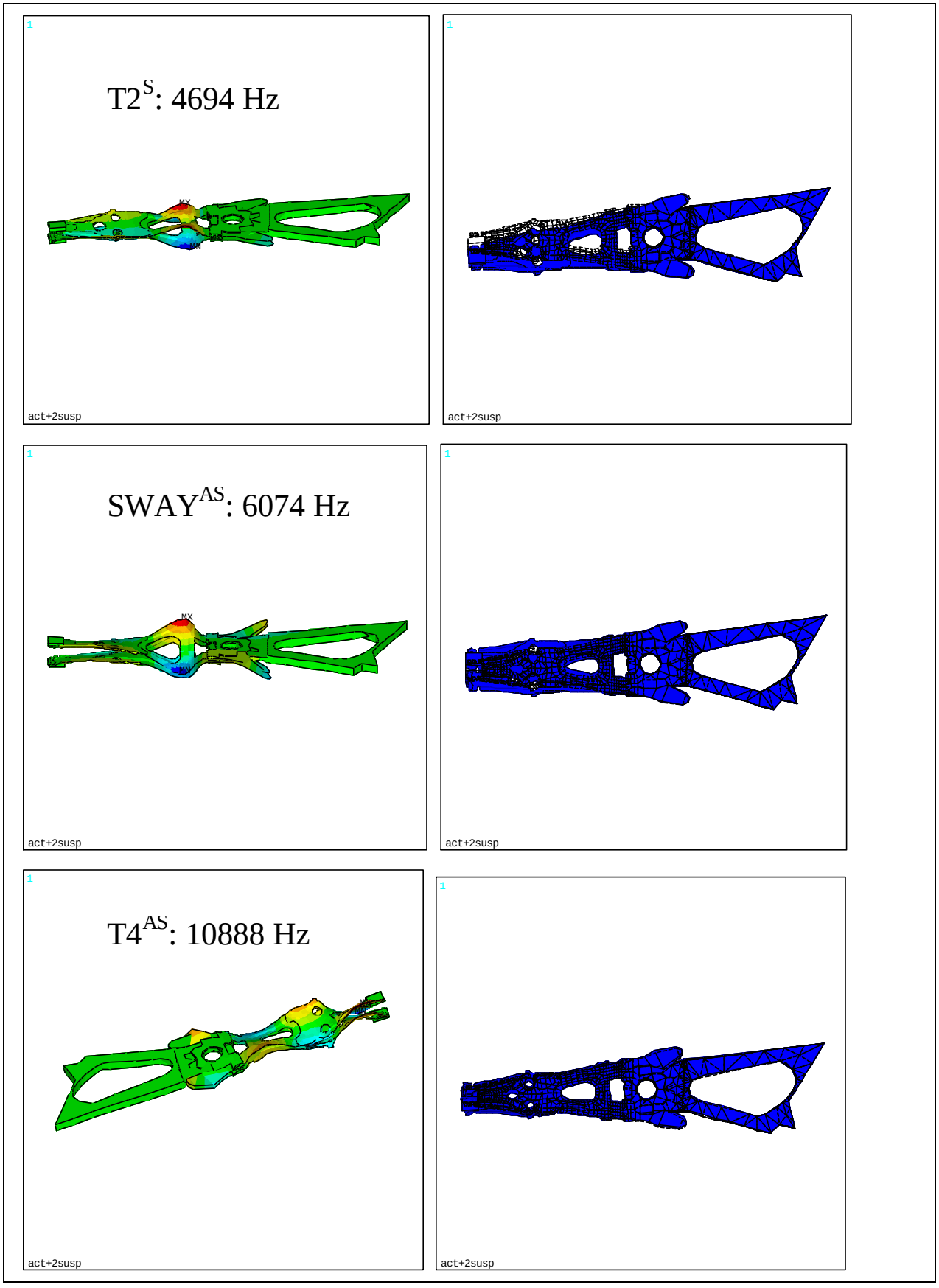

Figure 13: Modes contributing to off-track motion for the 2AS arm-suspension system.

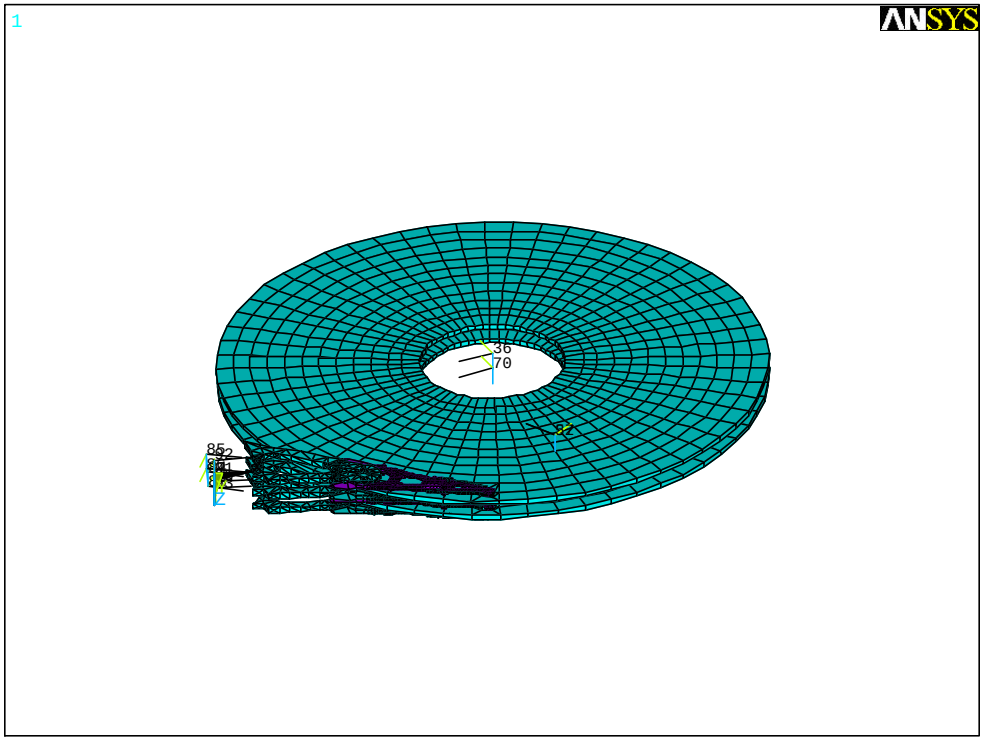

Figure 14: FE model of the disk drive.

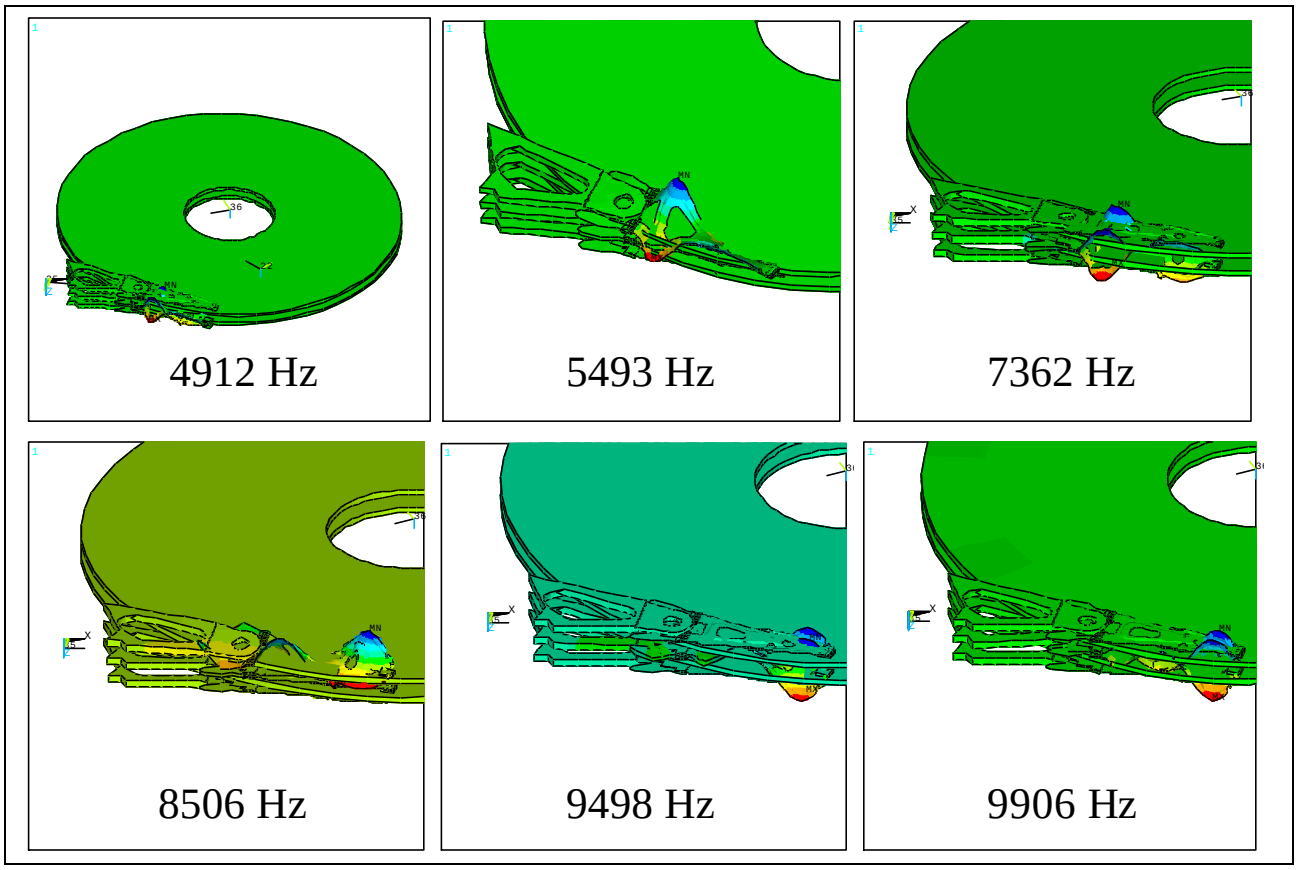

Figure 15: Mode shapes contributing to off-track motion.

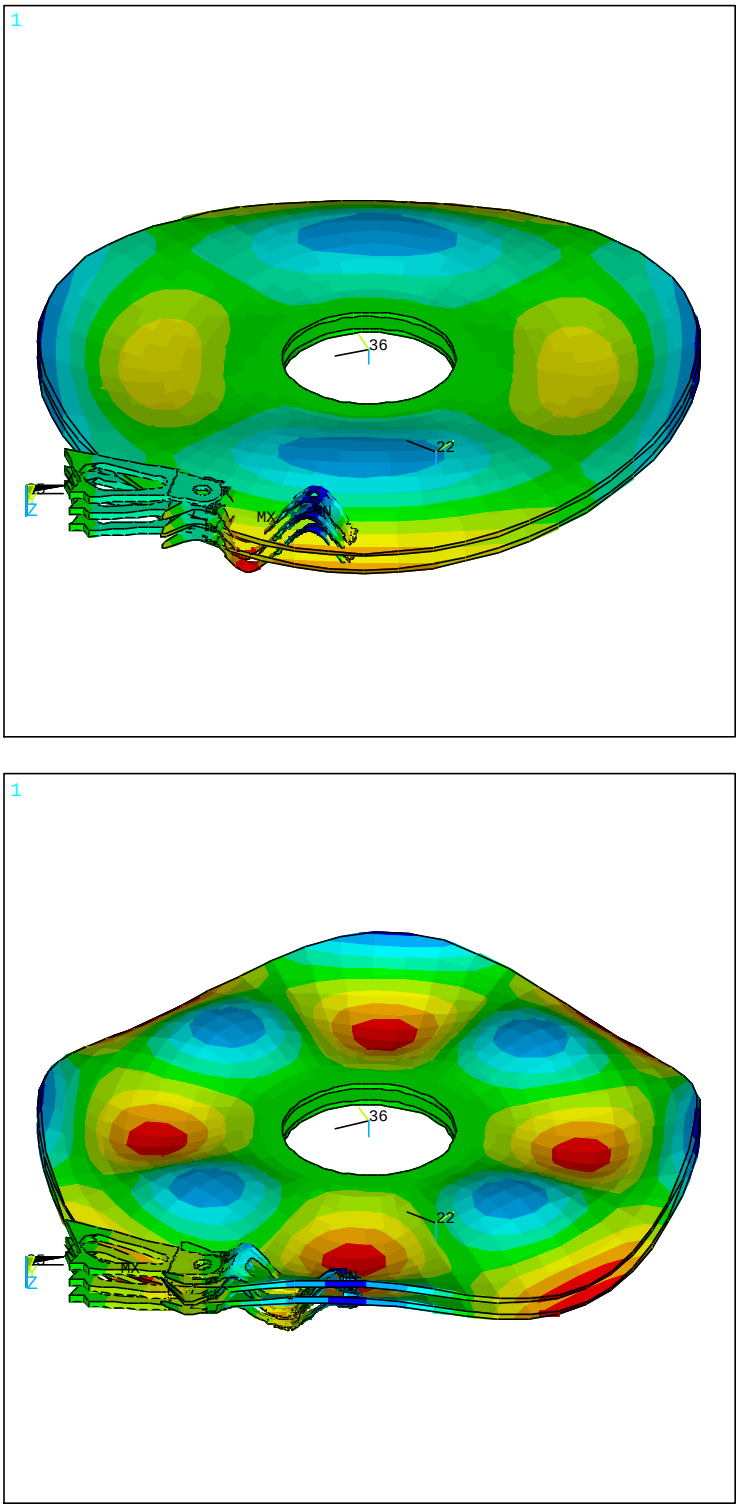

Figure 16: Two representative FE coupled modes for stationary disks.

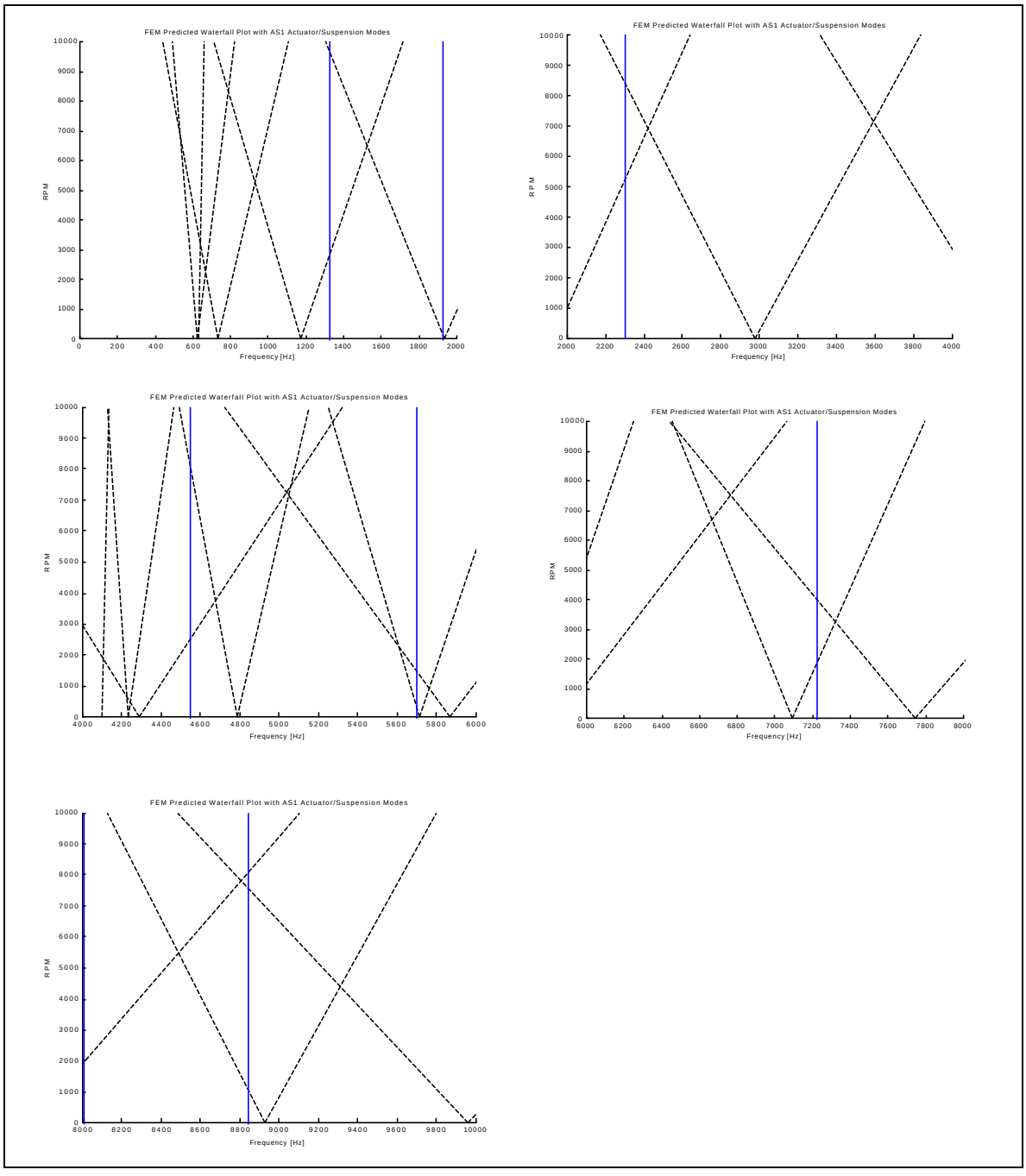

Figure 17: Finite element predicted waterfall plot for disk modes and 1AS modes.

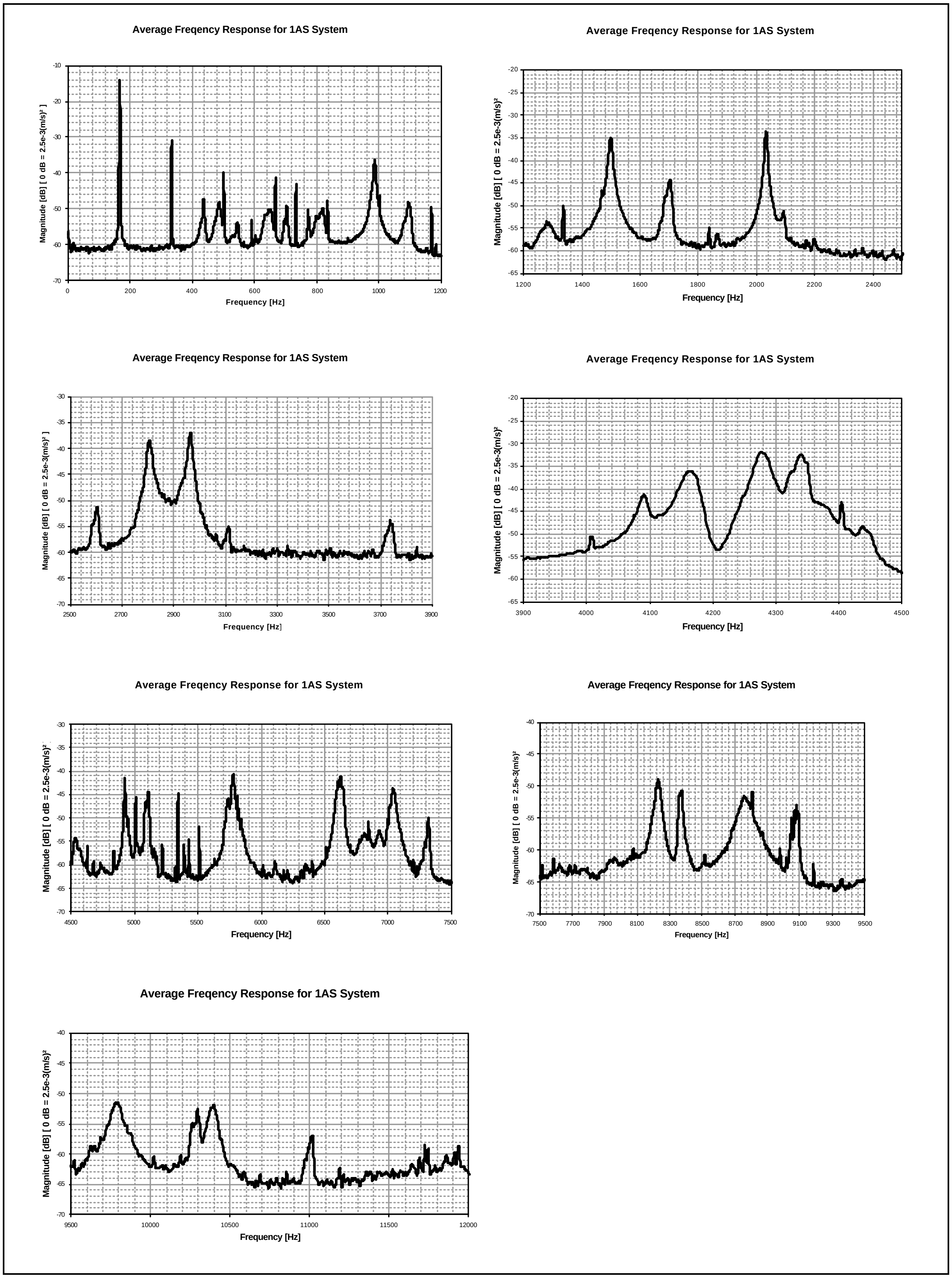

Figure 18: Modal analysis frequency response averaged 32 times for the 1AS system.

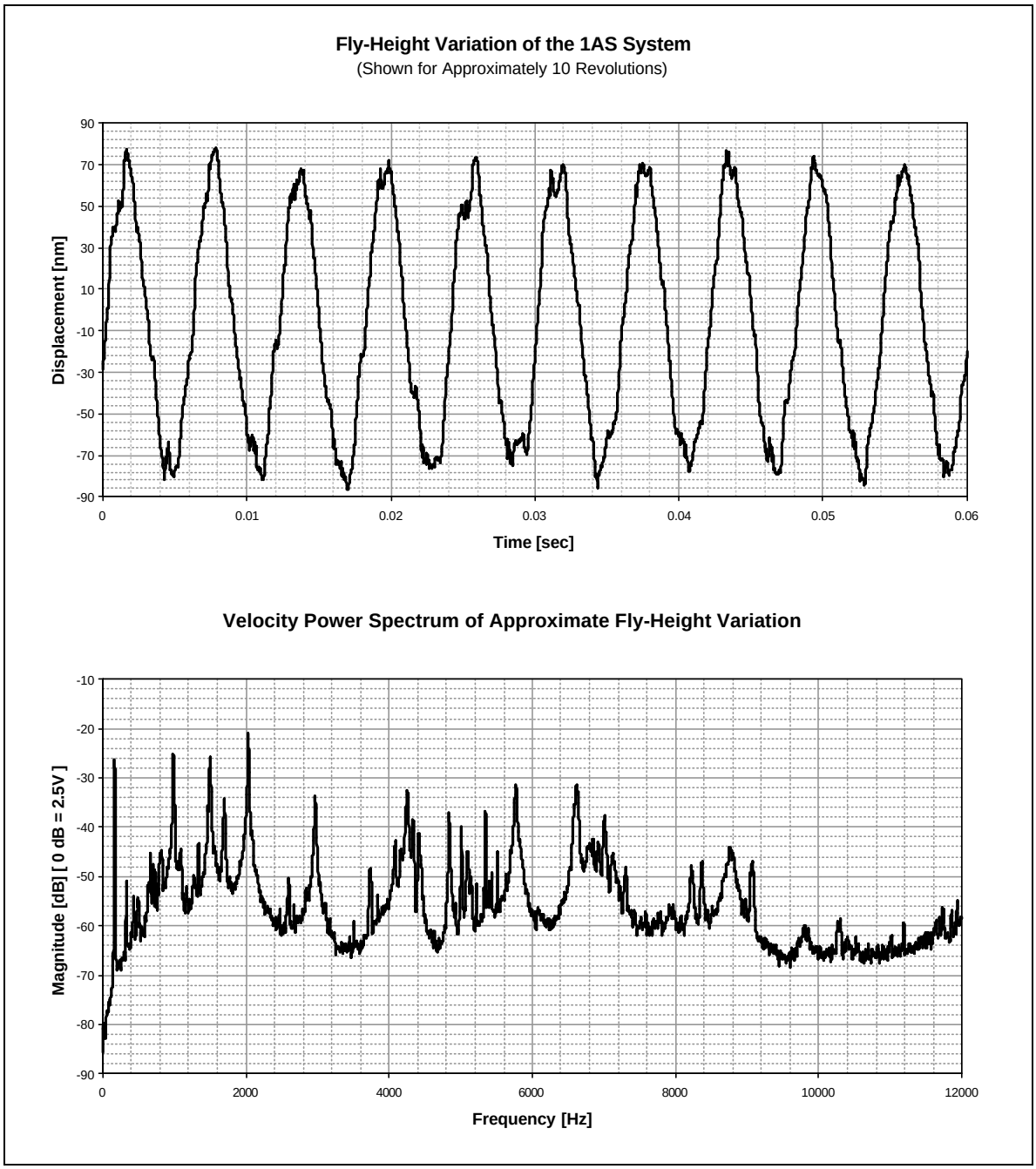

Figure 19: Approximate fly-height modulation of the 1AS system. Both time and frequency domain data shown.

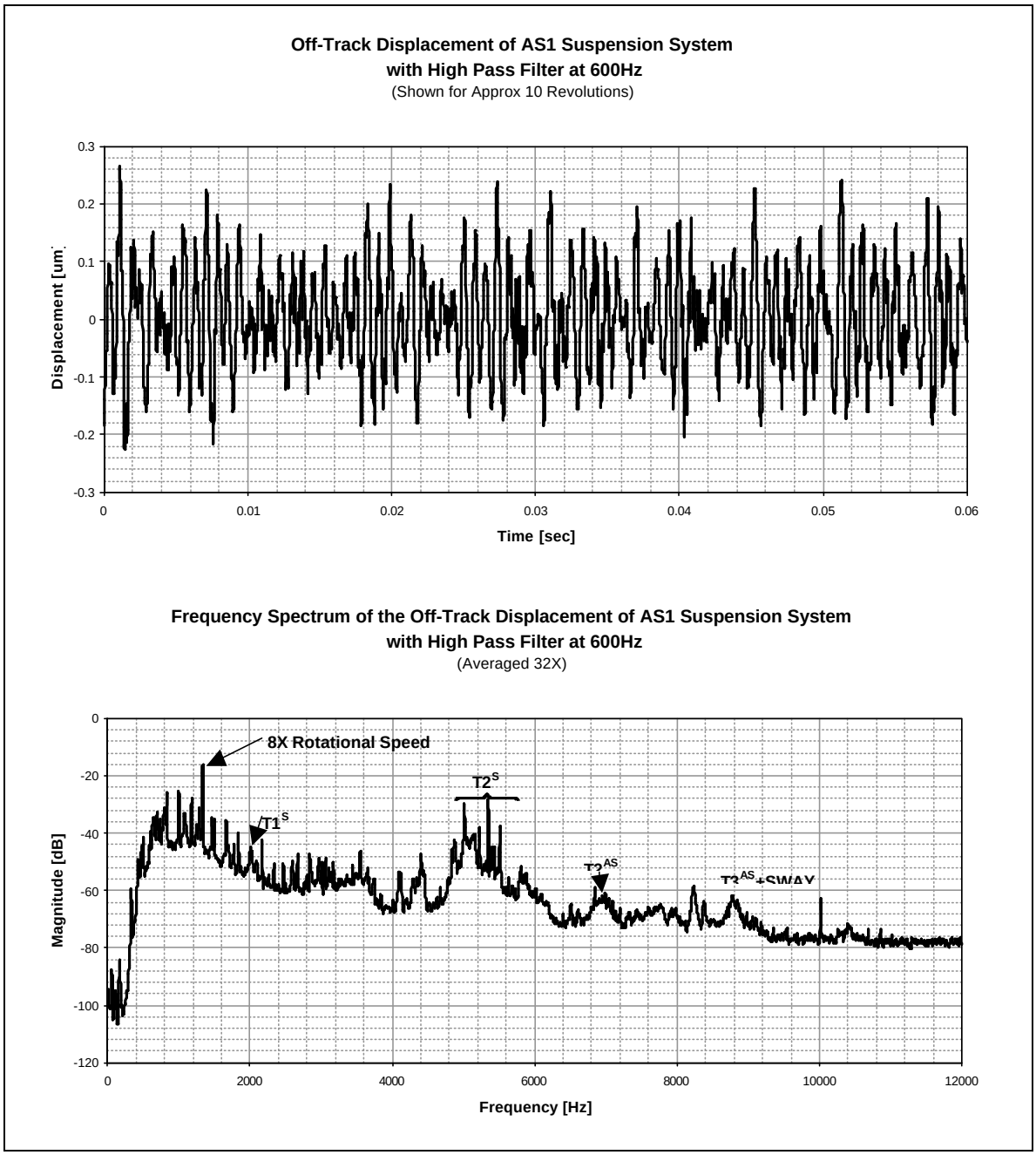

Figure 20: Off-track displacement of the 1AS slider in the time and frequency domain.

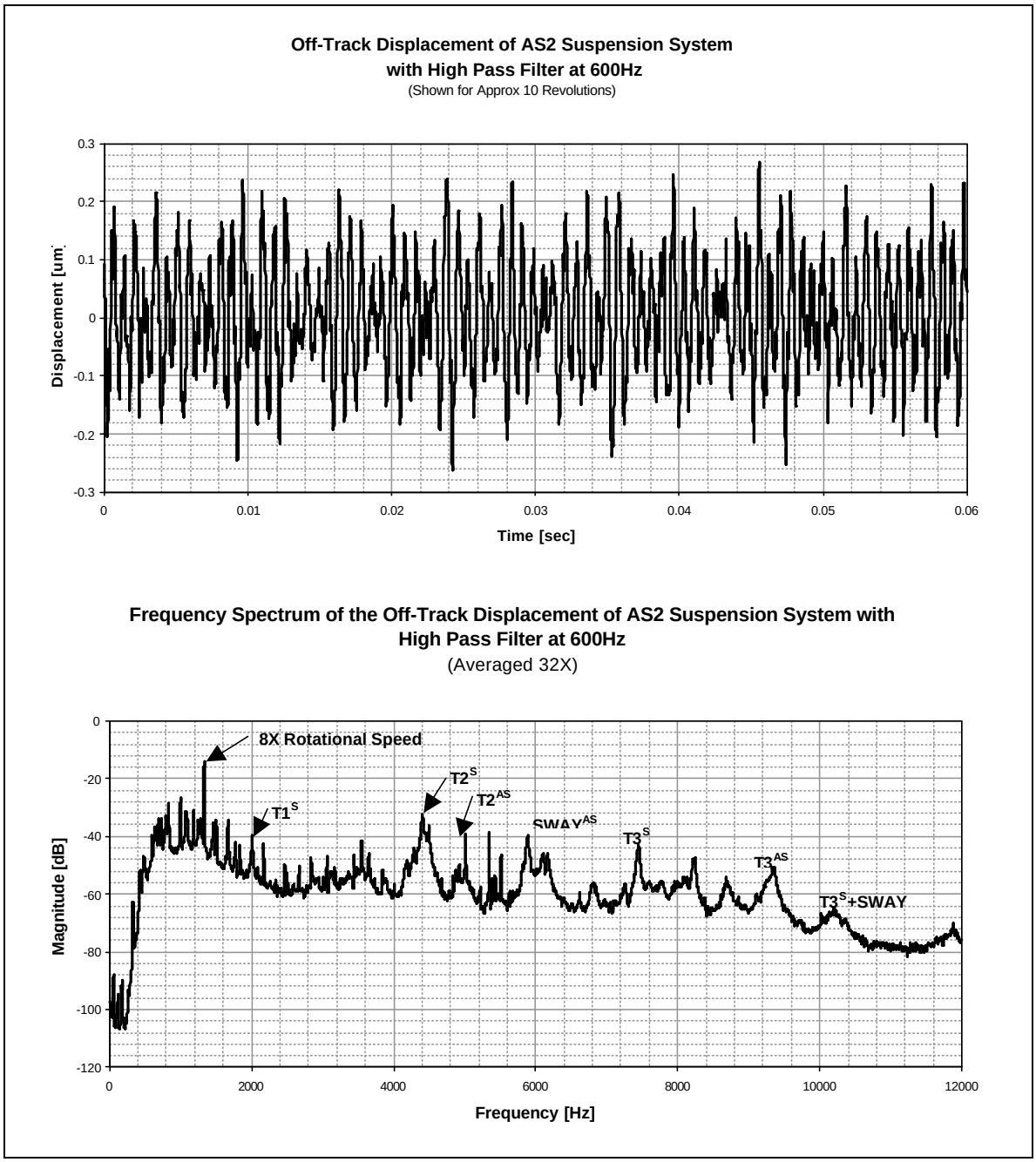

Figure 21: Off-track displacement of the 2AS system in the time and frequency domain.

Drive Specifications	
Spindle Speed:	10,020 RPM
Number of Disks:	5
Form Factor Height:	1.6 inches
Number of Heads:	10
Ball-bearing spindle motor	
Aluminum substrate 95 mm disks	

Table 1: HDD specifications.

Mode Shape	FE Analysis Frequency [Hz]	Experimental Frequency [Hz]	% Error
B1	1432	1300	10.2
T1	2319	2087	11.1
Tabs Flap^{+}	3490	--	--
Tabs Flap^{-}	3491	--	--
B2	4445	4406	0.9
T2	6135	6300	2.6
B3	8297	8412	1.4
T3	9467	--	---
Sway	11377	11725	3.0
Gimble	11915	--	--

Table 2: Summary of mode shapes and frequencies for FEA and experimental modal analysis with the percent error for the suspension-slider system. Highlighted modes are contributors to off-track motion.

Mode Shape	FEM Frequency [Hz]	Experimental Frequency [Hz]	Percent Error
B1	2359.7	2269	4.0
B2^{od}	8933.2	9150	2.4
B2^{id}	11872.9	10300	15.3
SWAY	13170.4	--	--

Table 3: Summary of mode shapes and frequencies for FEA and experimental modal analysis with the percent error for the actuator arm.

	Finite Element Mode Frequencies from FE Analysis	Prestress Mode Frequency from FE Analysis	Stiffening Increase	Predicted Traveling Modes	
				Forward	Backward
Mode Shape	**Frequency [Hz]**	**Frequency [Hz]**	**Frequency [Hz]**	**Frequency [Hz]**	**Frequency [Hz]**
$(0,1)^2$	622.8	657.6	34.8	824.3	491.0
(0,0)	629.6	659.0	29.3	-	-
$(0,2)^2$	732.6	776.0	43.4	1109.3	442.6
$(0,3)^2$	1169.0	1210.9	41.9	1710.9	710.9
$(0,4)^2$	1933.3	1970.6	37.3	2637.2	1303.9
$(0,5)^2$	2974.9	3008.7	33.8	3842.0	2175.3
(1,0)	4101.5	4133.5	32.0	-	-
$(1,1)^2$	4263.3	4295.4	32.1	4462.0	4128.7
$(0,6)^2$	4285.8	4317.3	31.5	5317.3	3317.3
$(1,2)^2$	4790.1	4823.0	33.0	5156.3	4489.7
$(1,3)^2$	5714.2	5747.4	33.2	6247.4	5247.4
$(0,7)^2$	5865.3	5894.8	29.5	7061.4	4728.1
$(1,4)^2$	7090.9	7124.2	33.4	7790.9	6457.5
$(0,8)^2$	7745.0	7772.9	27.9	9106.2	6439.6
$(1,5)^2$	8931.1	8964.2	33.1	9797.5	8130.8
$(0,9)^2$	9959.2	9986.2	27.0	11486.2	8486.2
?	11193.0	11194.0	1.0	-	-
$(1,6)^2$	11229.5	11262.0	32.5	12262.0	10262.0
(2,0)	12247.0	12279.0	32.0	-	-
$(2,1)^2$	12448.5	12481.0	32.5	12647.7	12314.3
$(0,10)^2$	12550.0	12575.5	25.5	14242.2	10908.8
$(2,2)^2$	13074.0	13106.0	32.0	13439.3	12772.7

Table 4: FEA predicted mode shapes and frequencies for a stationary and rotating disk at 10,000 RPM (highlighted values are the predicted modes at 10,000 RPM).

Mode Shape	FE Analysis Disk Modes for Stationary Disk Frequency [Hz]	Experimentally Found Disk Modes Frequency [Hz]	Percent Error
$(0,1)^2$	622.8	618	**0.8**
(0,0)	629.6	630	**0.1**
$(0,2)^2$	732.6	712.5	**2.8**
$(0,3)^2$	1169.0	1137.5	**2.8**
$(0,4)^2$	1933.3	1875	**3.1**
$(0,5)^2$	2974.9	2850	**4.4**
(1,0)	4101.5	4037.5	**1.6**
$(1,1)^2$	4263.3	4062.5	**4.9**
$(0,6)^2$	4285.8	4212.5	**1.7**
$(1,2)^2$	4790.1	4712.5	**1.6**
$(1,3)^2$	5714.2	5412.5	**5.6**
$(0,7)^2$	5865.3	5575	**5.2**
$(1,4)^2$	7090.9	7012.5	**1.1**
$(0,8)^2$	7745.0	7625	**1.6**
$(1,5)^2$	8931.1	8750	**2.1**

Table 5: FEA compared with experiment with the percent error for a stationary disk. Percent error is highlighted.

1AS Suspension System	
Mode Shape	Frequency [Hz]
$B1^{AS}$	1322
$B2^{AS}$	1923
$T1^{S}$	2304
$B3^{AS}$	4548
$T2^{S}$	5699
$T2^{AS}$	7221
$B4^{AS}$	8012
$T3^{AS}$+SWAY	8848
$T+B2^{odA}$	10062
$T+B2^{idA}$	10458
Gimble	11909
$B4^{S}$	12741

2AS Suspension System	
Mode Shape	Frequency [Hz]
$B1^{AS}$	1095
$B1^{S-}$	1428
$B2^{AS}$	1691
$T1^{S+}$	2266
$T1^{S-}$	2310
$B2^{S-}$	4400
$B2^{S+}$	4527
$T2^{S-}$	4694
$T2^{AS+}$	5285
$Sway^{AS+}$	6074
$T3^{S-}$	7269
$B4^{AS+}$	7405

(Cont.)

2AS Suspension System	
Mode Shape	Frequency [Hz]
$B3^{S-}$	8197
$T3^{AS+}$	9116
$B5^{AS+}$	9433
$T3^{S-}$	9958
$T3+Sway^{A}$	10395
$T4^{AS+}$	10888
$Gimble^{-}$	11826
$Gimble^{+}$	11930

Table 6: Mode shapes and frequencies of the 1AS & 2AS suspension-slider systems. Highlighted modes contribute to off-track motion.

Mode Shape	Frequency [Hz]
$(0,1)^{+S}$	619
$(0,1)^{-S}$	619.2
$(0,1)^{+}$	622.9
$(0,1)^{-}$	622.9
$(0,0)^{+}$	628.4
$(0,0)^{-}$	628.4
$(0,2)^{S+}$	728
$(0,2)^{S-}$	728.3
$(0,2)^{+}$	733.4
$(0,2)^{-}$	733.4
$B1^{AS+/2S}$	1087.2
$(0,3)^{-}B1^{S-/2S}B1^{AS-/1S}$	1154.8
$(0,3)^{+}B1^{AS+/1S}B1^{AS+/2S}$	1162.6
$(0,3)^{-}$	1168.7
$(0,3)^{+}$	1168.7
$B1^{AS-/1S}$	1269.7
$B1^{AS+/1S}$	1270.8
$B1^{S-/2S}$	1439.5
$B2^{AS+/2S}$	1681.5
$B2^{AS-/1S}$	1791.4
$B2^{AS+/1S}$	1791.5
$(0,4)^{-}$	1930.4
$(0,4)^{+}$	1930.4
$(0,4)^{-}B2^{AS-/1S}B1^{S-/2S}$	1944.6
$(0,4)^{+}B2^{AS+/1S}B2^{AS+/2S}$	1947
$T1^{S+/2S}$	2275
$T1^{S/1S}$	2292.7
$T1^{S/1S}$	2292.7
$T1^{S-/2S}$	2313.6
$(0,5)^{-}$	2968.2
$(0,5)^{+}$	2968.2
$(0,5)^{-}B1^{S-/1S}B1^{S-/2S}$	2978.9
$(0,5)^{+}B1^{S+/1S}B1^{S+/2S}$	2979.2

Mode Shape (cont.)	Frequency [Hz] (cont.)
$(1,0)^{-}B2^{S-/1S}B2^{S-/2S}$	4097
$(1,0)^{+}B2^{S+/1S}B2^{S+/2S}$	4097.8
$(1,1)^{-}B2^{S-/1S}B2^{S-/2S}$	4239.9
$(1,1)^{+}B2^{S+/1S}B2^{S+/2S}$	4246.4
$(1,1)^{-}$	4261
$(1,1)^{+}$	4261
$(0,6)^{-}$	4276.2
$(0,6)^{+}$	4276.2
$(0,6)^{-}B2^{S-/1S}B2^{S-/2S}$	4286.8
$(0,6)^{+}B2^{S+/1S}B2^{S+/2S}$	4288
$B2^{S-/1S}B2^{S-/2S}$	4439
$B2^{S+/1S}B2^{S+/2S}$	4522.1
$B3^{AS-/1S}B2^{S-/2S}$?	4533.4
$B3^{AS+/1S}B3^{AS+/2S}$	4546
$(1,2)^{-}B3^{S-/1S}B2^{S-/2S}$	4789.1
$(1,2)^{+}B3^{S+/1S}B3^{S+/2S}$	4789.8
$(1,2)^{-}$	4795.8
$(1,2)^{+}$	4795.8
SWAY $T2^{S+/2S}$	4912.3
$T2^{AS/2S}$	5438.1
$T2^{S/1S}$	5493.3
$T2^{S/1S}$	5496.6
$(1,3)^{+}B2^{S+/1S}B2^{S+/2S}$	5702.9
$(1,3)^{-}B2^{S-/1S}B2^{S-/2S}$	5703.1
$(1,3)^{-}$	5723.8
$(1,3)^{+}$	5723.8
$(0,7)^{+}$	5847.9
$(0,7)^{-}$	5847.9
$(0,7)^{+}B2^{S+/1S}B2^{S+/2S}$	5878.6
$(0,7)^{-}B2^{S-/1S}B2^{S-/2S}$	5878.9
$Sway^{AS+/2S}$	6261.9
$T2^{AS/1S}$	6262.5
$T2^{AS/1S}$	6265.1

Mode Shape (cont.)	Frequency [Hz] (cont.)
$(1,4)^{+}B4^{AS+/1S}B4^{AS+/2S}$	7066.5
$(1,4)^{-}B4^{AS-/1S}B3^{S-/2S}$	7067.8
$(1,4)^{+}$	7109.1
$(1,4)^{-}$	7109.1
$B2^{A}T2^{S-/2S}$	7362.4
$B4^{AS+/2S}$	7425.5
$(0,8)^{-}B4^{AS-/1S}$	7664.6
$(0,8)^{-}B4^{AS-/1S}$	7690
$(0,8)^{-}B4^{AS-/1S}$	7716
$(0,8)^{-}B4^{AS-/1S}B3^{S-/2S}$	7787.5
$(0,8)^{+}B4^{AS+/1S}B4^{AS+/2S}$	7802.3
$B3^{S-/2S}$	8256.7
$T3^{AS/1S}$	8460.1
$T3^{AS/1S}$	8505.9
$(1,5)^{+}B5^{AS+/1S}B5^{AS+/2S}$	8900.9
$(1,5)^{-}B5^{AS-/1S}B4^{S-/2S}$	8905.1
$(1,5)^{+}$	8956.7
$(1,5)^{-}$	8956.7
$B4^{AS+/2S}$	9289.4
$B2^{odA}T2^{S+/2S}B?^{S}$	9497.8
$B2^{odA}T2^{S+/1S}B?^{S}$	9587.6
$B2^{odA}T2^{S+/1S}B?^{S}$	9588.9
$SWAY^{A}T3^{S-/2S}$	9906.3
$(0,9)^{+}$	9917
$(0,9)^{-}T3^{S-/2S}$	9917.6
$(0,9)^{-}B5^{AS-/1S}B4^{S-/2S}$	10001
$(0,9)^{+}B5^{AS+/1S}B5^{AS+/2S}$	10004
$T4^{AS/1S}$	10263
$T4^{AS/1S}$	10297
$T3^{S-/2S}$	10538
$T4^{AS+/2S}$	11378
$SWAY^{A}T3^{S1/S}$	11472
$SWAY^{A}T3^{S1/S}$	11520

Table 7: Summary of mode shapes and frequencies for the FEA of the disk drive system. The highlighted modes are contributors to off-track motion.

Mode Number	Frequency [Hz]	Mode Shape
1	167.5	Fundamental Disk Rotation
2	333.8	2 Times Fundamental Disk Rotation
3	436.3	$(0,2)^{-}$
4	486.3	$(0,1)^{-}$
5	543.8	?
6	652.5	(0,0)
7	702.5	$(0,3)^{-}$
8	818.8	$(0,1)^{+}$
9	986.3	$B1^{AS}$
10	1095	$B1^{AS}(0,2)^{+}$
11	1278	$B1^{AS}(0,4)^{-}$
12	1500	$B2^{AS}$
13	1701	$B2^{AS}(0,3)^{+}$
14	2031	T1
15	2094	$T1(0,5)^{-}$
16	2603	$(0,4)^{+}$
17	2806	FLAP
18	2962	FLAP+B
19	3112	$(0,6)^{-}$
20	3737	$B3^{AS}(0,5)^{+}$
21	4091	$B3^{AS}$
22	4166	$B3^{AS}$
23	4278	$B3^{AS}$
24	4341	$(0,7)^{-}B3^{AS}$
25	4403	$B3^{AS}$
26	4438	$B3^{AS}$
27	4513	?
28	4628	$B3^{AS}$
29	4838	$B1^{A}T2^{S}$
30	4922	$B1^{A}T2^{S}$
31	5009	$(0,6)^{+}B1^{A}B2^{S}$
32	5084	DISK ?
33	5109	$B3^{AS}$
34	5156	$T2^{S}$
35	5219	$T2^{S}$
36	5344	$T2^{S}$
37	5391	$T2^{S}$

(cont.)

Mode Number	Frequency [Hz]	Mode Shape
38	5428	T2S
39	5509	T2S
40	5737	(0,8)-T?
41	5781	T2S
42	6109	T2S
43	6628	(0,7)+T?
44	6816	T2S
45	6931	T2S
46	7041	B4AS
47	7291	(0,9)-B4AS
48	7319	(0,9)-
49	8228	T3AS+SWAY
50	8359	(0,8)+
51	8375	B?(0,8)+
52	8759	B?
53	9050	DISK B
54	9069	DISK B
55	9081	DISK B
56	9794	Sflap
57	10260	Sflap Disk
58	10290	"
59	10390	Sflap
60	11020	DISK
61	12360	DISK+B4S
62	13130	?
63	13440	?
64	14930	T?

*Drive in operational state on LBA 0 (OD Track)
Input: LDV on screw holding the actuator to the base plate.
Output: Scanning LDV on the Top suspension+ actuator system.

Table 8: Experimental modal analysis of the 1AS suspension system under normal operation (OD track following).

Mode Shape	FE Predicted Frequency [Hz]	Experimentally Found Frequency [Hz]
$B1^{AS}(0,2)^{+}$	1110	1095
$B1^{AS}(0,4)^{-}$	1304	1278
$B2^{AS}(0,3)^{+}$	1711	1701
$B2^{AS}(0,5)^{-}$	2175	--
$B3^{AS}(0,5)^{+}$	3842	3737
$B3^{AS}(1,1)$	4462	--
$B3^{AS}(1,2)^{-}$	4490	--
$B3^{AS}(0,7)^{-}$	4728	4341
$B4^{AS}(1,5)^{-}$	8131	--
$B4^{AS}(0,9)^{-}$	8486	7291
$B4^{AS}(1,4)^{+}$	7791	--

Table 9: FE predicted coupled modes frequency compared with experimentally found coupled modes.